GABAergic neuron-to-glioma synapses in diffuse midline gliomas

Tara Barron[1], Belgin Yalçın[1], Aaron Mochizuki[1], Evan Cantor[2], Kiarash Shamardani[1],

Dana Tlais[1], Andrea Franson[2], Samantha Lyons[2], Vilina Mehta[1], Samin Maleki Jahan[1],

Kathryn R. Taylor[1], Michael B. Keough[1], Haojun Xu[1], Minhui Su[1], Michael A. Quezada[1],

Pamelyn J Woo[1], Paul G. Fisher[1], Cynthia J. Campen[1], Sonia Partap[1], Carl Koschmann[2],

Michelle Monje[1,3,*]

1 Department of Neurology and Neurological Sciences, Stanford University, Stanford CA 94305 USA

2 Department of Pediatric Hematology/Oncology, University of Michigan, Ann Arbor Michigan USA

3 Howard Hughes Medical Institute, Stanford University, Stanford CA 94305 USA

*Please send correspondence to: Michelle Monje MD PhD (mmonje@stanford.edu)

Abstract

Pediatric high-grade gliomas are the leading cause of brain cancer-related death in children. High-grade gliomas include clinically and molecularly distinct subtypes that stratify by anatomical location into diffuse midline gliomas (DMG) such as diffuse intrinsic pontine glioma (DIPG) and hemispheric high-grade gliomas. Neuronal activity drives high-grade glioma progression both through paracrine signaling[1,2] and direct neuron-to-glioma synapses[3-5]. Glutamatergic, AMPA receptor-dependent synapses between neurons and malignant glioma cells have been demonstrated in both pediatric[3] and adult high-grade gliomas[4], but neuron-to-glioma synapses mediated by other neurotransmitters remain largely unexplored. Using whole-cell patch clamp electrophysiology, *in vivo* optogenetics and patient-derived glioma xenograft models, we have now identified functional, tumor-promoting GABAergic neuron-to-glioma synapses mediated by $GABA_A$ receptors in DMGs. GABAergic input has a depolarizing effect on DMG cells due to NKCC1 expression and consequently elevated intracellular chloride concentration in DMG tumor cells. As membrane depolarization increases glioma proliferation[3], we find that the activity of GABAergic interneurons promotes DMG proliferation *in vivo*. Increasing GABA signaling with the benzodiazepine lorazepam – a positive allosteric modulator of $GABA_A$ receptors commonly administered to children with DMG for nausea or anxiety - increases $GABA_A$ receptor conductance and increases glioma proliferation in orthotopic xenograft models of DMG. Conversely, levetiracetam, an anti-epileptic drug that attenuates GABAergic neuron-to-glioma synaptic currents, reduces glioma proliferation in patient-derived DMG xenografts and extends survival of mice bearing DMG xenografts. Concordant with gene expression patterns of $GABA_A$ receptor subunit genes across subtypes of glioma, depolarizing GABAergic currents were not found in hemispheric high-grade gliomas. Accordingly, neither lorazepam nor levetiracetam influenced the growth rate of hemispheric high-grade glioma patient-derived xenograft models. Retrospective real-world clinical data are consistent with these conclusions and should be replicated in future prospective clinical studies. Taken together, these findings uncover GABAergic synaptic communication between GABAergic interneurons and diffuse midline glioma cells, underscoring a tumor subtype-specific mechanism of brain cancer neurophysiology with important potential implications for commonly used drugs in this disease context.

Introduction

Diffuse midline glioma (DMG), which occurs most commonly in the brainstem and is also known as diffuse intrinsic pontine glioma (DIPG), is a lethal childhood central nervous system cancer with few therapeutic options and a median survival of only 10-13 months[6,7]. The majority of DMGs exhibit a mutation in genes encoding histone H3 (H3K27M), and occur in the brainstem, thalamus and spinal cord[8-10]. Multiple lines of evidence support

57   the concept that DMG originates from oligodendroglial lineage precursor cells[11-15]. During

58   postnatal development and adulthood, oligodendroglial precursor cells (OPCs)

59   communicate with neurons through both paracrine factor signaling[16-18] and through

60   glutamatergic and GABAergic neuron-to-OPC synapses[19-23]; oligodendroglial precursor

61   cell proliferation is robustly regulated by neuronal activity[24]. Similar to these effects on

62   their normal cellular counterparts, glutamatergic neuronal activity drives the proliferation

63   and growth of DMG and other high-grade[1,4,25,26] and low-grade[2] gliomas. The

64   mechanisms by which neuronal activity promotes glioma progression include activity-

65   regulated paracrine factor secretion[1,2,25,26] as well as electrochemical communication

66   through AMPA (α-amino-3-hydroxy-5-methyl-4-isoxazole propionic acid) receptor

67   (AMPAR)-mediated neuron-to-glioma synapses[3,4] and activity-dependent, potassium-

68   evoked glioma currents that are evident in both pediatric and adult forms of high-grade

69   gliomas[3,4]. Depolarizing current alone is sufficient to drive malignant glioma growth in

70   orthotopic xenograft models [3], underscoring the need for a comprehensive understanding

71   of electrochemical mechanisms that enable glioma membrane depolarization in each

72   molecularly distinct form of glioma. Here, we explore whether GABAergic synapses exist

73   between GABAergic interneurons and DMG cells and test the hypothesis that putative

74   GABAergic synaptic signaling is depolarizing and promotes tumor progression in

75   H3K27M-altered DMG.

76

77   **Results**

78   **GABA$_A$ receptor and postsynaptic gene expression in DMG**

79   To determine whether genes involved in GABAergic synaptic transmission are

80   expressed in high-grade gliomas, we analyzed single-cell RNAseq datasets from primary

81   patient tumor samples of H3K27M+ DMG cells, IDH wild-type (WT) hemispheric high-

82   grade glioma cells, IDH mutant (mut) hemispheric high-grade glioma cells, and tumor-

83   associated non-malignant oligodendrocytes (OLs). H3K27M+ DMG cells broadly

84   expressed GABA$_A$ receptor subunit genes, including α and β subunits, as well as

85   ARHGEF9, GPHN, and NLGN2, which are associated with GABAergic post-synaptic

86   regions (Figure 1a). These genes were expressed to a much greater extent in H3K27M+

87   DMG cells than in IDH WT high-grade gliomas (Figure 1a).

88

89   **Functional GABAergic neuron-glioma synapses**

90   To determine whether putative functional GABAergic neuron-glioma synapses

91   exist, we performed electrophysiological recordings from xenografted H3K27M+ DMG

92   cells in response to stimulation of local GABAergic interneurons. Green fluorescent

93   protein (GFP)-expressing glioma cells were xenografted into the CA1 region of the

94   hippocampus, a well-defined circuit in which neuron-to-glioma synapses have been

95   previously reported[3] and allowed to engraft and grow for at least 8 weeks. Acute

96   hippocampal sections were prepared from these mice, and DMG cell responses to

97   electrical stimulation of local neurons with a bipolar stimulator were recorded using whole-

98   cell patch clamp electrophysiology (Figure 1b). Using a high Cl$^-$ internal solution and in

99   the presence of AMPAR antagonist NBQX (2,3-dihydroxy-6-nitro-7-sulfamoyl-

100   benzo[f]quinoxaline) to inhibit AMPAR-mediated currents, local stimulation led to an

101   inward current in DMG cells recorded in voltage clamp (Figure 1c). This current was

102   blocked with perfusion of picrotoxin (PTX), a $GABA_A$ receptor inhibitor, indicating that

103   these synaptic currents are mediated by GABA. GABAergic neuron-to-glioma synapses

104   were observed in two distinct patient-derived xenograft models (Figure 1d). Cells were

105   filled with Alexa Fluor 568 dye during electrophysiological recording and then slices were

106   post-fixed, immunostained for tumor cell markers [GFP and human nuclear antigen

107   (HNA)] and imaged on a confocal microscope to confirm that the cells recorded from were

108   glioma cells (Figure 1e).

109

110   **GABA depolarizes DMG cells due to NKCC1-mediated high intracellular Cl⁻**

111         $GABA_A$ receptor activation can either depolarize or hyperpolarize a cell, depending

112   on the intracellular Cl^- concentration. In mature neurons, Cl^- concentration is low, leading

113   to an influx of Cl^- through $GABA_A$ receptors and thus, hyperpolarization [27]. OPCs exhibit

114   a high intracellular Cl^- concentration, leading to an efflux of Cl^- through $GABA_A$ receptors,

115   and thus GABAergic neuron-to-OPC synapses cause depolarization[20]. Perforated patch

116   recordings of xenografted H3K27M+ DMG cells using gramicidin-A revealed that local

117   application of GABA induced an inward current in voltage clamp and corresponding

118   depolarization in current clamp (Figure 2a-b). The effect of local GABA application on

119   H3/IDH WT pediatric hemispheric glioblastoma (pGBM) was negligible in comparison

120   (Figure 2a-b). PTX inhibited the current and depolarization in response to GABA

121   application, indicating that $GABA_A$ receptors are responsible for this depolarizing effect.

122   To determine the reversal potential of $GABA_A$ currents (E_{GABA}) in H3K27M+ DMG and

123   H3/IDH WT pGBM xenografts, we recorded response to local GABA application at varying

124   holding potentials (Figure 2c). The currents in response to GABA were plotted against the

125 holding potentials, and E_{GABA} was found to be -19.61 ± 8.29 mV and -14.14 ± 9.04 mV for

126 H3K27M+ DMG cells from two different patient-derived models (SU-DIPGVI and SU-

127 DIPGXIII-FL, respectively) and -47.44 ± 7.79 mV for H3/IDH WT pGBM (Figure 2d;

128 Extended Data Figure 1). Using these reversal potentials to calculate the intracellular Cl⁻

129 concentration of each glioma type, we find the intracellular Cl⁻ concentration of H3K27M+

130 DMG cells to be 62.65 mM in SU-DIPGVI cells and 76.88 mM in SU-DIPGXIII-FL cells,

131 and that of H3/IDH WT pGBM to be 22.12 mM. During whole-cell recordings with high Cl⁻

132 internal solution, the reversal potential was -0.41 ± 12.98 mV in H3K27M+ DMG cells,

133 illustrating the critical role of chloride concentration gradients.

134   Cation–chloride cotransporters, such as the Na-K-Cl cotransporter NKCC1, have

135 an important role in setting intracellular Cl⁻ concentration. *SLC12A2*, the gene that

136 encodes for NKCC1, is expressed in H3K27M+ DMG (Figure 2e). To determine the role

137 of NKCC1 in E_{GABA} in DMG cells, we used perforated patch to record the response to

138 local GABA application in the presence of bumetanide, an NKCC1 inhibitor. After bath

139 perfusion of bumetanide, E_{GABA} was shifted from -19.61 ± 8.29 mV to -54.20 ± 8.19 mV

140 in H3K27M+ DMG cells (Figure 2f), a value similar to that found in H3/IDH WT pGBM

141 cells (Figure 2d) indicating that NKCC1 function is critical for the depolarizing effect of

142 GABA on these cells.

143

144 **GABAergic interneurons increase DMG proliferation**

145   Past work has demonstrated that glutamatergic neuronal activity promotes glioma

146 progression[1-5], and that depolarization of glioma cells plays a central role in these effects

147 of neuronal activity on glioma proliferation[3]. Since GABA has a depolarizing effect on

148   DMG cells as described above, we sought to determine whether GABAergic interneurons

149   drive DMG proliferation through depolarizing GABAergic synaptic input. We first used

150   whole-cell patch clamp electrophysiology to confirm that we could perform optogenetic

151   and pharmacological targeting of GABAergic neuron-to-glioma synapses. We genetically

152   expressed ChRmine, a red-shifted channelrhodopsin[28], in Dlx-expressing GABAergic

153   interneurons in the CA1 region of the hippocampus and recorded the response of

154   xenografted glioma cells to 5 ms optogenetic stimulation of those neurons (Figure 3a).

155   PTX-sensitive GABAergic post-synaptic currents in DMG cells were observed in response

156   to optogenetic interneuron stimulation (Figure 3b). We also observed the tetrodotoxin

157   (TTX)-sensitive prolonged currents, evoked by activity-dependent extracellular K^+

158   increase, that we have previously described[3] (Figure 3b). Whole cell patch clamp

159   recordings of Dlx-ChRmine-expressing interneurons confirmed that optogenetic

160   stimulation evoked depolarization (Extended Data Figure 2a). Pharmacological targeting

161   of GABAergic neuron-to-glioma synaptic input using a benzodiazepine, lorazepam, which

162   increases conductance of $GABA_A$ receptors, increased the amplitude of GABAergic post-

163   synaptic currents in DMG cells (Figure 3c-e).

164   We next sought to test the effect of interneuron activity and GABAergic synaptic

165   input into DMG cells *in vivo*. Dlx-ChRmine was expressed in hippocampal interneurons

166   via AAV viral vector injection to the CA1 region, and *in vivo* optogenetic stimulation of

167   interneuron activity was confirmed by expression of the immediate early gene cFos

168   (Extended Data Figure 2b). Eleven weeks after injection of Dlx-ChRmine vector into the

169   hippocampus, and eight weeks after xenografting patient-derived H3K27M+ DMG cells

170   to the same area, the CA1 region of the hippocampus was optogenetically stimulated

171 (595 nm light, 40 Hz, 30 sec on/90 sec off over 30 minutes) in awake, behaving mice to

172 stimulate GABAergic interneuron activity (Figure 3f). Control mice were identically

173 manipulated, but light was not delivered during mock optogenetic stimulation. The

174 thymidine analogue EdU was administered systemically to mice at the time of optogenetic

175 or mock stimulation to label proliferating cells, and glioma cell proliferation was analyzed

176 24-hours later. *In vivo* optogenetic stimulation of GABAergic interneurons promoted

177 proliferation of xenografted DMG cells (Figure 3g). Similarly, treatment of xenografted

178 mice with lorazepam, which increases $GABA_A$ receptor signaling, exerted a dose-

179 dependent proliferative effect on H3K27M+ DMG in each of three independent patient-

180 derived orthotopic xenograft models (Figure 3h-j). While the effect of lorazepam was most

181 robust at high doses (8 mg/kg), in each xenograft model a significant dose-dependency

182 was evident with ANOVA post-test for linear contrast. The microenvironment of the brain,

183 such as the presence of GABAergic neurons, is required for the proliferative effect of

184 lorazepam, as no effect of lorazepam was observed in H3K27M+ DMG monocultures

185 (Extended Data Figure 3a). As expected, given the lack of GABA-induced currents in

186 H3/IDH WT gliomas, lorazepam did not increase glioma proliferation in mice bearing

187 patient-derived H3/IDH WT pGBM xenografts (Extended Data Figure 4).

188

189 **Therapeutic potential of targeting GABAergic neuron-glioma synapses**

190 As neuron-glioma synapses robustly promote glioma cell proliferation and tumor

191 progression, identifying pharmacological treatments that target these synapses has high

192 therapeutic potential. Levetiracetam, a generally well-tolerated anti-epileptic drug with

193 multiple mechanisms of action, reduces GABAergic post-synaptic currents in DMG cells

194 (Figure 4a-b). Strikingly, mice bearing H3K27M+ DMG xenografts treated with

195 levetiracetam exhibited longer survival than vehicle-treated controls (Figure 4c).

196 Levetiracetam treatment decreased glioma proliferation in mice bearing H3K27M+ DMG

197 xenografts compared to vehicle-treated controls, an effect observed in three independent

198 patient-derived orthotopic xenograft models of H3K27M+ DMG (Figure 4d-f). The effect

199 of levetiracetam on glioma proliferation is dependent on the brain microenvironment

200 rather than cell-intrinsic effects, as no effect of levetiracetam was observed in H3K27M+

201 DMG monocultures (Extended Data Figure 3b).

202 Retrospective, real-world data from two major US pediatric neuro-oncology

203 centers (Stanford University and University of Michigan) was assessed to query possible

204 effects of levetiracetam on overall survival in pediatric patients with high-grade gliomas.

205 Kaplan-Meier analysis of all pHGG patients (n = 216) suggests a survival advantage of

206 levetiracetam usage (Extended Data Figure 5a). For multivariable survival analysis, we

207 utilized an elastic net-regularized Cox regression for variable selection and found that in

208 all patients with high-grade glioma, a diagnosis of DMG was – as expected - associated

209 with decreased overall survival (coefficient +0.55), and that thalamic DMG tumor location

210 (coefficient -0.20), and levetiracetam (coefficient -0.11) were associated with increased

211 overall survival; the variables of age, sex, ONC201 usage, and panobinostat usage had

212 coefficients of zero. Conventional or targeted chemotherapy other than ONC201 and

213 panobinostat were surprisingly associated with increased overall survival (coefficient -

214 0.61), which may be explained by the observation that pontine DMG subjects in the

215 historical database often did not receive any conventional or targeted therapy (Extended

216 Data Table 1) due to demonstrated lack of efficacy of conventional chemotherapy in

217   pontine DMG[29]. Hypothesizing that DMGs drove the positive survival association of

218   levetiracetam usage, we next evaluated DMG and hemispheric HGGs separately. These

219   databases include subjects with biopsy-demonstrated H3K27M-mutated or H3WT diffuse

220   midline gliomas as well as subjects prior to availability of molecular testing for whom

221   diagnosis was based only on the typical radiographic appearance of DMGs; both

222   H3K27M-altered and H3WT subgroups of DMGs are therefore included (Extended Data

223   Table 1). The DMG analysis suggests that patients with DMG who had a history of

224   levetiracetam usage (n = 15 children) exhibited a longer median overall survival (OS)

225   compared to those without levetiracetam usage (n = 105 children; Extended Data Figure

226   5b, Extended Data Table 1). Those DMG patients with a history of levetiracetam usage

227   had a median OS of 20.3 months, compared to those without levetiracetam usage who

228   exhibited a median OS of 9.2 months (P=0.025). Of note, thalamic DMG represented a

229   higher proportion of the group with a history of levetiracetam usage than the group with

230   no history of levetiracetam usage. Comparing subjects with thalamic and pontine DMG

231   who received levetiracetam, we find no difference in OS in this levetiracetam usage group

232   (Extended Data Figure 5c), suggesting that the higher proportion of thalamic DMG in this

233   group does not account for the observed increased median OS compared to the group

234   without levetiracetam usage. The median OS of the control (no levetiracetam usage)

235   group is consistent with the expected median OS for DIPG/DMG (10-11 months for

236   pontine DMG, 13 months for thalamic DMG)[6,7]. Important caveats are that these data are

237   retrospective, the numbers are small, and levetiracetam should be studied in future

238   prospective clinical studies with stratification by molecular subtype and DMG location

239   before drawing conclusions.

240   In contrast to the anti-proliferative effect of levetiracetam on xenografted H3K27M+

241   DIPG/DMG, levetiracetam treatment did not significantly affect glioma proliferation in mice

242   bearing patient-derived hemispheric (H3/IDH WT) high-grade glioma xenografts in three

243   independent models of pediatric and adult hemispheric H3/IDH WT glioblastoma (Figure

244   4g-i). Concordantly, analysis of the retrospective clinical data focused on hemispheric

245   pediatric high-grade gliomas revealed no effect of levetiracetam usage on OS in pediatric

246   patients with non-DMG, hemispheric high-grade gliomas (n=37, median OS 24.6 months

247   vs n=60 children, median OS 17.0 months with and without levetiracetam use,

248   respectively, P=0.74, Extended Data Figure 5d, Extended Data Table 2).

249   Phenytoin and ethosuximide, antiepileptic drugs that reduce neuronal

250   hyperexcitability but do not directly act on known mechanisms of neuron-to-glioma

251   communication, do not influence DMG proliferation *in vivo* or *in vitro* (Extended Data

252   Figure 6), highlighting the importance of specifically targeting neuron-to-glioma synapses.

253

254   **Discussion**

255   Glutamatergic neuronal activity has emerged as a powerful regulator of glioma

256   progression[2-4,25,26,30]. Across multiple clinically and molecularly distinct forms of pediatric

257   and adult gliomas, activity-regulated paracrine factors such as BDNF and shed neuroligin-

258   3 promote glioma growth [1,2,25,30]. Similarly, AMPAR-mediated glutamatergic synapses

259   drive progression in both H3K27M-altered DMG and hemispheric (H3/IDH WT)

260   glioblastomas[3,4]. Here, we demonstrate that GABAergic interneurons also promote

261   glioma progression through GABAergic synapses that are depolarizing and growth-

262   promoting in the specific disease context of diffuse midline gliomas. In contrast, only

263   minimal currents were found in the hemispheric (IDH/H3 WT) high-grade glioma models

264   used here; it is possible that some subtypes of hemispheric glioma may be found to

265   respond to GABA heterogenously[31]. We found that the commonly used anti-seizure drug

266   levetiracetam attenuates these GABAergic currents in diffuse midline gliomas, through

267   mechanisms that remain to be determined. Levetiracetam has multiple described

268   mechanisms, including binding to SV2A to decrease presynaptic release, but whether this

269   represents the mechanism operant in diminishing DMG GABA currents remains to be

270   tested in future studies. These discoveries highlight the therapeutic potential of re-

271   purposing levetiracetam to decrease GABAergic signaling in diffuse midline gliomas.

272

273   While this therapeutic potential is supported by the preclinical evidence and suggested

274   by the retrospective clinical data presented here, it is important to note that prospective

275   clinical trials are required to validate this effect. In this clinical retrospective study, it may

276   be that those subjects who developed seizures and therefore received levetiracetam had

277   tumors that are particularly neurotrophic and thus more susceptible to therapy with

278   levetiracetam. It is also possible that tumors growing in neuroanatomical locations with

279   relatively more GABAergic input or different GABA-dependent circuit dynamics are

280   differentially affected by levetiracetam therapy. An unknown confounder could also be

281   associated with levetiracetam therapy. Future work, studying larger numbers of patients

282   and stratifying subjects based on DMG location, molecular characteristics, and glioma

283   neuroscience correlative markers will be required to draw conclusions about the potential

284   role of levetiracetam for DMG therapy.

285

286   The anti-seizure drugs tested were growth-inhibitory only if the drug targeted specific

287   mechanisms of neuron-glioma interaction in that tumor type. Ethosuximide and phenytoin

288   do not target known mechanisms of neuron-glioma interactions and did not affect tumor

289   proliferation in the preclinical models used here. Similarly, neither levetiracetam nor

290   lorazepam influenced the proliferation of the three independent hemispheric (H3/IDH WT)

291   glioblastoma models used here. Past clinical studies of antiepileptic drug effects in adult

292   high-grade glioma have not been guided by knowledge of drugs that specifically target

293   neurophysiological mechanisms operant in that tumor type. Not surprisingly, the results

294   of such anti-seizure medication studies have been mixed. Levetiracetam used

295   concomitantly with chemoradiation has been reported to improve outcomes in

296   hemispheric, H3/IDH WT glioblastoma in some studies [32], while large meta-analyses have

297   found no discernable effect on outcome in others [33,34]. These discordant findings in the

298   literature may reflect the heterogeneity inherent in hemispheric H3/IDH WT high-grade

299   gliomas[34], and specific subgroups of H3/IDH WT glioblastoma yet-to-be determined could

300   be responsive to levetiracetam. Here, we found no effect of levetiracetam in three

301   independent preclinical models of pediatric and adult hemispheric (H3/IDH WT) high-

302   grade glioma and no effect of levetiracetam in retrospective analyses of pediatric patients

303   with non-DMG, hemispheric high-grade gliomas.

304

305   In DMGs, the risk to benefit ratio of benzodiazepines should be carefully considered.

306   Benzodiazepines, which potentiate signaling through $GABA_A$ receptors, promote glioma

307   GABAergic currents and tumor proliferation in the H3K27M-altered DMG models used

308   here. Benzodiazepines are commonly used in children with DMG for nausea, anxiety,

309   claustrophobia during MRI scans and other medical procedures, and for other reasons.

310   While benzodiazepines are important medications for palliative care, use should be

311   carefully considered in DMG outside of the context of end-of-life care and should be

312   further evaluated in clinical analyses. Conversely, and further underscoring differences

313   between DMG and hemispheric high-grade gliomas, preclinical studies indicate that

314   GABA and GABAergic interneurons may instead be growth-inhibitory hemispheric

315   (H3/IDH WT) adult glioblastoma models[35,36]. These findings underscore the therapeutic

316   importance of elucidating the neurophysiology of defined subtypes of brain cancers to

317   identify the patient populations for which a particular neurophysiological drug may be

318   beneficial or detrimental. Understanding the neuroscience of brain tumors will enable the

319   development of effective and safe therapeutic approaches, incorporating neuroscience-

320   informed therapies into combinatorial strategies targeting both cell-intrinsic and

321   microenvironmental mechanisms that drive progression of these devastating cancers.

322

323   **Methods**

324   **Human samples and data**

325   For all human tissue and cell studies, informed consent was obtained, and tissue was

326   used in accordance with protocols approved by the Stanford University Institutional

327   Review Board (IRB). IRB approval was also obtained for retrospective analyses of real-

328   world clinical data kept in IRB-approved databases at Stanford University and University

329   Michigan.

330

331   **Mice and housing conditions**

332   All *in vivo* experiments were conducted in accordance with protocols approved by the

333   Stanford University Institutional Animal Care and Use Committee (IACUC) and performed

334   in accordance with institutional guidelines. Animals were housed according to standard

335   guidelines with free access to food and water in a 12 h light:12 h dark cycle. For brain

336   tumor xenograft experiments, the IACUC does not set a limit on maximal tumor volume

337   but rather on indications of morbidity. In no experiments were these limits exceeded as

338   mice were euthanized if they exhibited signs of neurological morbidity or if they lost 15%

339   or more of their body weight.

340

341   **Orthotopic xenografting**

342   For all xenograft studies, NSG mice (NOD-SCID-IL2R gamma chain-deficient, The

343   Jackson Laboratory) were used. Male and female mice were used equally. A single-cell

344   suspension from cultured SU-DIPG-VI-GFP, SU-DIPG-XIII-FL-GFP, SU-DIPG-50-GFP,

345   SU-pcGBM2-GFP, SF0232, or SF0238 neurospheres were prepared in sterile PBS

346   immediately before the xenograft procedure. Animals at postnatal day (P) 28–30 were

347   anaesthetized with 1–4% isoflurane and placed in a stereotactic apparatus. The cranium

348   was exposed via midline incision under aseptic conditions. Approximately 300,000 cells

349   in 3 µl sterile PBS were stereotactically implanted through a 26-gauge burr hole, using a

350   digital pump at infusion rate of 0.4 µl min^{-1} and 26-gauge Hamilton syringe. For all

351   electrophysiology and optogenetics experiments, cells were implanted into the CA1

352   region of the hippocampus (1.5 mm lateral to midline, -1.8 mm posterior to bregma, −1.4

353   mm deep to cranial surface). SU-DIPG-XIII-FL-GFP for lorazepam and levetiracetam

354   treatments were xenografted into the premotor cortex (0.5 mm lateral to midline, 1.0 mm

355   anterior to bregma, −1.75 mm deep to cranial surface). SU-DIPG-XIII-P for survival study

356   and SU-DIPG-VI-GFP and SU-DIPG-50-GFP for lorazepam, levetiracetam,

357   ethosuximide, and phenytoin treatments were xenografted into the pons (1.0 mm lateral

358   to midline, −0.8 mm posterior to lambda, −5.0 mm deep to cranial surface). At the

359   completion of infusion, the syringe needle was allowed to remain in place for a minimum

360   of 2 min, then manually withdrawn at a rate of 0.875 mm min^{-1} to minimize backflow of

361   the injected cell suspension.

362

363   **Patient-derived cell culture**

364   All high-grade glioma cultures were generated as previously described [11]. In brief, tissue

365   was obtained from high-grade glioma (WHO (World Health Organization) grade III or IV)

366   tumors at the time of biopsy or from early post-mortem donations. Tissue was dissociated

367   both mechanically and enzymatically and grown in a defined, serum-free medium

368   designated 'tumor stem media' (TSM), consisting of neurobasal(-A) (Invitrogen), B27(-A)

369   (Invitrogen), human bFGF (20 ng ml^{-1}; Shenandoah), human EGF (20 ng ml^{-1};

370   Shenandoah), human PDGF-AA (10 ng ml^{-1}) and PDGF-BB (10 ng ml−1; Shenandoah)

371   and heparin (2 ng ml^{-1}; Stem Cell Technologies). For all patient-derived cultures,

372   mycoplasma testing was routinely performed, and short tandem repeat DNA fingerprinting

373   was performed every three months to verify authenticity. The short tandem repeat

374   fingerprints and clinical characteristics for the patient-derived cultures and xenograft

375   models used have been previously reported [37].

376

377   **Single-cell sequencing analysis**

378 We combined publicly available single-cell datasets processed and annotated

379 previously[13,38], all sequenced using smart-seq2 protocol. Following the quality-control

380 measures taken in these studies, we filtered the data to keep cells with more than 400

381 detected genes, and genes that were expressed in more than 3 cells. We assessed the

382 single-cell transcriptome from 6,341 adult IDH-mutant glioma cells derived from biopsies

383 from 10 study participants, 599 adult wild-type IDH glioma cells derived from biopsies

384 from 3 study participants, and 2,458 pediatric H3K27M DMG cells derived from biopsies

385 from 6 study participants, as well as the single-cell transcriptome of patient-derived SU-

386 DIPGVI and SU-DIPGXIII-FL cells. Malignant cells were inferred by expression programs

387 and detection of tumor-specific genetic alterations. For each sample, we performed first

388 cell-level normalization, and then centered the gene expression around 0 to allow

389 principal component analysis (PCA) computation. Following the PCA reduction, we

390 clustered the cells using shared nearest neighbor clustering. To examine the various

391 GABA$_A$ receptor signatures of each of the cells in each cluster, we used the function

392 AddModuleScore by Seurat package, which calculates the average expression levels of

393 the gene set subtracted by the aggregated expression of 100 randomly chosen control

394 gene sets, where the control gene sets are chosen from matching 25 expression bins

395 corresponding to the tested gene set expression. The gene sets used are as followed:

396 GABA$_A$ receptor α: GABRA1, GABRA2, GABRA3, GABRA4, GABRA5, GABRA6; GABA$_A$

397 receptor β: GABRB1, GABRB2, GABRB3; total GABA$_A$ receptor: GABRA1, GABRA2,

398 GABRA3, GABRA4, GABRA5, GABRA6, GABRB1, GABRB2, GABRB3, GABRG1,

399 GABRG2, GABRG3, GABRD, GABRE, GABRP, GABRQ, GABRR1, GABRR2,

400 GABRR3.

401

Slice preparation for electrophysiology

Coronal slices (300 µm thick) containing the hippocampal region were prepared from mice

(at least 8 weeks after xenografting) in accordance with a protocol approved by Stanford

University IACUC. After rapid decapitation, the brain was removed from the skull and

immersed in ice-cold slicing artificial cerebrospinal fluid (ACSF) containing (in mM): 125

NaCl, 2.5 KCl, 25 glucose, 25 NaHCO$_3$ and 1.25 NaH$_2$PO$_4$, 3 MgCl$_2$ and 0.1 CaCl$_2$. After

cutting, slices were incubated for 30 min in warm (30 °C) oxygenated (95% O2, 5% CO2)

recovery ACSF containing (in mM): 100 NaCl, 2.5 KCl, 25 glucose, 25 NaHCO$_3$, 1.25

NaH$_2$PO4, 30 sucrose, 2 MgCl$_2$ and 1 CaCl$_2$ before being allowed to equilibrate at room

temperature for an additional 30 min.

412

Electrophysiology

Slices were transferred to a recording chamber and perfused with oxygenated, warmed

(28–30 °C) recording ACSF containing (in mM): 125 NaCl, 2.5 KCl, 25 glucose, 25

NaHCO$_3$, 1.25 NaH$_2$PO$_4$, 1 MgCl$_2$ and 2 CaCl$_2$. NBQX (10 µM) was perfused with the

recording ACSF to prevent AMPA receptor-mediated currents in synaptic response

experiments. TTX (0.5 µM) was perfused with the recording ACSF to prevent neuronal

action potential firing in GABA puff experiments. Slices were visualized using a

microscope equipped with DIC optics (Olympus BX51WI). Recording patch pipettes (3-5

MΩ) were filled with CsCl-based pipette solution containing (in mM): 150 CsCl, 5 EGTA,

1 MgCl$_2$, 10 HEPES, 2 ATP, 0.3 GTP, pH = 7.3. Pipette solution additionally contained

Alexa 568 (50 µM) to visualize the cell through dye-filling during whole-cell recordings.

424   Gramicidin A (60 μg/mL) was added to the pipette solution for perforated patch

425   recordings. Glioma cells were voltage-clamped at −70 mV. Synaptic responses were

426   evoked with a bipolar electrode connected to an Iso-flex stimulus isolator (A.M.P.I.)

427   placed near the xenografted cells. GABA (1 mM) in recording ACSF was applied via a

428   puff pipette, which was placed approximately 100 μm away from the patched cell and

429   controlled by a Picospritzer II (Parker Hannifin Corp.). Optogenetic currents were evoked

430   with a 598 nm LED using a pE-4000 illumination system (CoolLED). Signals were

431   acquired with a MultiClamp 700B amplifier (Molecular Devices) and digitized at 10 kHz

432   with an InstruTECH LIH 8+8 data acquisition device (HEKA). Data were recorded and

433   analyzed using AxoGraph X (AxoGraph Scientific) and IGOR Pro 8 (Wavemetrics). For

434   representative traces, stimulus artifacts preceding the synaptic currents have been

435   removed for clarity. Intracellular chloride concentration was calculated using the Nernst

436   equation.

437

438   **Inhibitors**

439   Drugs and toxins used for electrophysiology were picrotoxin (50 μM; Tocris), TTX (0.5

440   μM; Tocris), NBQX (10 μM; Tocris), bumetanide (100 μM), lorazepam (10 μM; Hospira),

441   and levetiracetam (100 μM; Selleck Chemicals). When used for *in vitro* slice application,

442   drugs were made up as a stock in distilled water or dimethylsulfoxide (DMSO) and

443   dissolved to their final concentrations in ACSF before exposure to slices.

444

445   **Viral injection and fibre optic placement**

446   Animals were anesthetized with 1-4% isoflurane and placed in a stereotaxic apparatus.

447   For optogenetic stimulation experiments, 1 µl of AAV8-Dlx5/6-ChRmine::oScarlet (virus

448   titer= 1.19x1012) (a gift from Dr. Karl Deisseroth from Stanford University; Chen et al.,

449   2020, Nature Biotech) was unilaterally injected using Hamilton Neurosyringe and

450   Stoelting stereotaxic injector over 5 minutes. The viral vector was injected into

451   hippocampus CA1 in the right hemisphere at coordinates: 1.5 mm lateral to midline, -1.8

452   mm posterior to bregma, -1.3 mm deep to cranial surface. 2 weeks following the viral

453   injection, SU-DIPG-XIII-FL cells were xenografted as described above. After 7 weeks of

454   tumor engraftment, an optic ferrule was placed above the CA1 of the hippocampus of the

455   right hemisphere, at 1.5 mm lateral to midline, -1.8 mm posterior to bregma, -1.25 mm

456   deep to cranial surface.

457

458   **Optogenetic stimulation**

459   Optogenetic stimulations were performed at least 10 weeks after the viral vector delivery,

460   8 weeks after xenografts, and 1 week after optic ferrule implantation. Freely moving

461   animals were connected to a 595 nm fiber-coupled LED laser system with a monofiber

462   patch cord. Optogenetic stimulation was performed with cycles of 595 nm light pulses at

463   40 Hz frequency, 10 ms width, and a light power output of 10-15mW from the tip of the

464   optic fiber, which lasted for 30 seconds, followed by 90 seconds recovery over a 30-

465   minute period. Animals were injected intraperitoneally with 40 mg/kg EdU (5-ethynyl-2'-

466   deoxyuridine; Invitrogen, E10187) before the session, and were perfused 24 hours after

467   the optogenetic stimulations.

468

469 **Bioluminescence imaging**

470 For in vivo monitoring of tumor growth, bioluminescence imaging was performed using

471 an IVIS imaging system (Xenogen). Mice orthotopically xenografted with luciferase-

472 expressing glioma cells were placed under isofluorane anesthesia and injected with

473 luciferin substrate. Animals were imaged at baseline and randomized based on tumor

474 size by a blinded investigator so that experimental groups contained an equivalent range

475 of tumor sizes. Over the course of each study (described below), all total flux values were

476 then normalized to baseline values to determine fold change of tumor growth.

477

478 **Mouse drug treatment studies**

479 For all drug studies, NSG mice were xenografted as above with SU-DIPG-VI-GFP, SU-

480 DIPG-XIII-FL-GFP, SU-DIPG-50-GFP, SU-pcGBM2-GFP, SF0232, or SF0238 cells and

481 randomized to treatment group by a blinded investigator. Four to six weeks post-

482 xenograft, mice were treated with systemic administration of lorazepam (8 mg kg^{-1} or 2

483 mg kg^{-1}; Hospira), levetiracetam (20 mg kg^{-1}; Selleck Chemicals), or phenytoin (50 mg

484 kg^{-1}; Selleck Chemicals) via intraperitoneal injection, or ethosuximide (300 mg kg^{-1};

485 Selleck Chemicals) via oral gavage for four weeks (5 days per week). For all studies,

486 controls were treated with an identical volume of the relevant vehicle. Bioluminescence

487 imaging was performed before treatment and every 7 days thereafter using an IVIS

488 imaging system (Xenogen) under isoflurane anesthesia. Tumor burden was assessed as

489 fold change in total flux from the beginning to end of treatment.

490

491 **Xenograft survival studies**

492   For survival studies, morbidity criteria used were either reduction of weight by 15% initial

493   weight, or severe neurological motor deficits consistent with brainstem dysfunction (that

494   is, hemiplegia or an incessant stereotyped circling behavior seen with ventral midbrain

495   dysfunction). Kaplan–Meier survival analysis using log rank testing was performed to

496   determine statistical significance.

497

498   **Perfusion and immunohistochemistry**

499   Animals were anaesthetized with intraperitoneal avertin (tribromoethanol), then

500   transcardially perfused with 20 ml of PBS. Brains were fixed in 4% PFA overnight at 4 °C,

501   then transferred to 30% sucrose for cryoprotection. Brains were then embedded in

502   Tissue-Tek O.C.T. (Sakura) and sectioned in the coronal plane at 40 μm using a sliding

503   microtome (Microm HM450; Thermo Scientific).

504

505   For immunohistochemistry, coronal sections were incubated in blocking solution (3%

506   normal donkey serum, 0.3% Triton X-100 in TBS) at room temperature for 2 hours.

507   Chicken anti-GFP (1:500, Abcam), mouse anti-human nuclei clone 235-1(1:100;

508   Millipore), or rabbit anti-Ki67 (1:500; Abcam) were diluted in antibody diluent solution (1%

509   normal donkey serum in 0.3% Triton X-100 in TBS) and incubated overnight at 4 °C.

510   Sections were then rinsed three times in TBS and incubated in secondary antibody

511   solution containing Alexa 488 donkey anti-chicken IgG, Alexa 594 donkey anti-rabbit IgG,

512   or Alexa 647 donkey anti-mouse IgG used at 1:500 (Jackson Immuno Research) in

513   antibody diluent at 4 °C overnight. Sections were rinsed three times in TBS and mounted

514   with ProLong Gold Mounting medium (Life Technologies).

515

Confocal imaging and quantification of cell proliferation

Cell quantification within xenografts was performed by a blinded investigator using live counting on a 40× oil immersion objective or 20× air objective of a Zeiss LSM700 or Zeiss LSM800 scanning confocal microscope and Zen imaging software (Carl Zeiss). For Ki67 analysis, 3 fields for quantification were selected from each of 3 consecutive sections in a 1-in-6 series of 40-µm coronal sections with respect to overall tumor burden. Within each field, all HNA-positive and GFP-positive tumor cells were quantified to determine tumor burden within the areas quantified. HNA-positive were then assessed for co-labelling with Ki67. To calculate the proliferation index (the percentage of proliferating tumor cells for each mouse), the total number of HNA-positive cells co-labelled with Ki67 across all areas quantified was divided by the total number of cells counted across all areas quantified (Ki67+/HNA+).

528

EdU Incorporation Assay

Diffuse intrinsic pontine glioma (DIPG) tumor neurosphere cultures SU-DIPGVI, SU-DIPGXIII, and SU-DIPG50 were generated as previously described[3,7] from early post-mortem tissue donations and grown as tumor neurospheres in defined, serum-free 'tumor stem media' (TSM) media, consisting of 1:1 mixture of neurobasal(-A) (Invitrogen) and D-MEM/F-12 (Invitrogen), HEPES buffer (Invitrogen), MEM sodium pyruvate (Invitrogen), MEM non-essential amino acids (Invitrogen), GlutaMAX-1 supplement (Invitrogen), B27(-A) (Invitrogen), human bFGF (20 ng/ml; Shenandoah), human EGF (20 ng/ml;

537 Shenandoah), human PDGF-AA (10 ng/ml) and PDGF-BB (10 ng/ml; Shenandoah) and

538 heparin (2 ng/ml; Stem Cell Technologies).

539

540 100,000 glioma cells were plated onto circular glass coverslips (Electron Microscopy

541 Services) pre-treated for 1 h at 37 °C with poly-L-lysine (Sigma) and then 1 h at 37 °C

542 with 10 µg/ml natural mouse laminin (Thermo Fisher). Dimethyl sulfoxide (Sigma-Aldrich)

543 or drugs at the concentrations indicated (dissolved in dimethyl sulfoxide) were added to

544 the coverslips. 10 µM EdU was added to each coverslip. Cells were fixed after 24 hr using

545 4% paraformaldehyde in PBS and stained using the Click-iT EdU kit and protocol

546 (Invitrogen). Proliferation index was then determined by quantifying the fraction of EdU

547 labeled cells/DAPI labeled cells using confocal microscopy.

548

549 **Retrospective, real-world patient data**

550 Retrospective data on patients with high-grade glial tumors were collected from patient

551 databases at Stanford University (1990-2020) and the University of Michigan (2012-2021)

552 through protocols approved by the respective institutional review boards. Database

553 source data for pediatric high-grade glioma patients were reviewed for this study to

554 ensure veracity and completeness. Overall survival was calculated using the Kaplan-

555 Meier estimator; the log-rank test was utilized to compare survival distributions. Patients

556 were censored at time of last contact for the Kaplan-Meier analysis. Given the number of

557 potential parameters with high correlation, an elastic net-regularized regression was

558 utilized for covariate selection in a multivariable survival model. Clinical data including

559 age; sex; tumor location; diagnosis of DMG; and administration of ONC201, panobinostat,

560   conventional chemotherapy, and levetiracetam were considered potential covariates.

561   Twenty-fold cross-validation was used to obtain the value of λ that gave the minimum

562   mean cross-validated error; corresponding coefficients for each variable were

563   subsequently determined. All data were compiled and analyzed in R version 4.0 or

564   higher.

565

566   **Statistical analyses**

567   Statistical tests were conducted using Prism (GraphPad) software unless otherwise

568   indicated. Gaussian distribution was confirmed by the Shapiro–Wilk normality test. For

569   parametric data, unpaired two-tailed Student's t-tests or one-way ANOVA with Tukey's

570   post hoc tests to examine pairwise differences were used as indicated. Paired two-tailed

571   Student's t-tests were used in the case of same cell experiments (as in

572   electrophysiological recordings). For non-parametric data, a two-sided unpaired Mann–

573   Whitney test was used as indicated, or a one-tailed Wilcoxon matched-pairs signed rank

574   test was used in the case of same-cell experiments. Two-tailed log rank analyses were

575   used to analyze statistical significance of Kaplan–Meier survival curves. A level of $P <$

576   0.05 was used to designate significant differences. Based on the variance of xenograft

577   growth in control mice, we used at least three mice per genotype to give 80% power to

578   detect an effect size of 20% with a significance level of 0.05. For all mouse experiments,

579   the number of independent mice used is listed in figure legend. Statistical analyses of

580   retrospective patient data are described above.

581

582   **Data availability**

583   All data are available in the manuscript or from the corresponding author upon reasonable

584   request. Source data will be uploaded with the final version of the manuscript.

585

586   **Code availability**

587   Sources for all code used have been provided, no custom code was created for this

588   manuscript.

589

599

600   **Author contributions:** M.M. and T.B. designed the experiments and wrote the

601   manuscript. T.B., B.Y., K.S. V.M., S.M.J., K.R.T, M.B.K., H.X., M.S., M.A.Q., and P.J.W

602   conducted experiments and performed data analyses. P.G.F., S.P., C.J.C., A.M., C.K.,

603   D.L. maintained patient databases at Stanford and University of Michigan; A.M., E.C.,

604   A.F., S.L., abstracted data from the databases; D.T. and C.K. reviewed source data for

605   all pediatric high-grade glioma database entries to ensure veracity and completeness.

606   All authors contributed to manuscript editing. M.M. conceived the project and

607   supervised all aspects of the work.

608

609   **Author declarations:** M.M. holds equity in MapLight Therapeutics and Syncopation

610   Life Sciences.

611

612
613

614

Figure 1. GABAergic neuron-glioma synapses.

a. Single cell RNAseq analysis of primary human biopsies of H3K27M diffuse midline glioma (grey; n = 2,259 cells, 6 study participants), IDH wild-type (WT) high-grade glioma (blue; n = 599 cells, 3 participants), IDH mutant (mut) high-grade glioma (purple; n = 5,096 cells, 10 participants) malignant cells, and tumor-associated, non-malignant oligodendrocytes (OL, yellow; n = 232 cells), demonstrating expression of total GABA$_A$ receptor subunit genes, α subunit genes, β subunit genes, and postsynaptic genes

622   specific to GABAergic synapses. Statistical analyses performed on single cells are

623   represented with stars only when also significant when analyzed on a per patient basis

624   as well as a per cell basis. Comparisons to OL (control cell type) are not shown.

625   **b.** Patient-derived DMG cells expressing GFP were xenografted into the CA1 region of

626   the hippocampus of NSG mice. Response to local CA1 stimulation via a bipolar stimulator

627   was recorded in xenografted cells using whole-cell patch clamp electrophysiology.

628   **c.** Representative trace of picrotoxin (PTX)-sensitive GABAergic postsynaptic current

629   (PSC) in a DMG cell (left). Quantification of current amplitude after 50 μM PTX as a % of

630   control (right; n = 7 cells from 5 mice). Recording performed in the presence of NBQX to

631   block AMPAR currents.

632   **d.** Representative traces of GABAergic PSCs in two xenografted DMG cell lines.

633   **e.** Confocal image of a xenografted DMG cell dye-filled (Alexa 568; red) during recording

634   and co-labelled with GFP (green) and HNA (white) post-recording. Scale bar, 10 μm. All

635   data are mean ± s.e.m. ****$P < 0.0001$, paired Student's t-test.

636
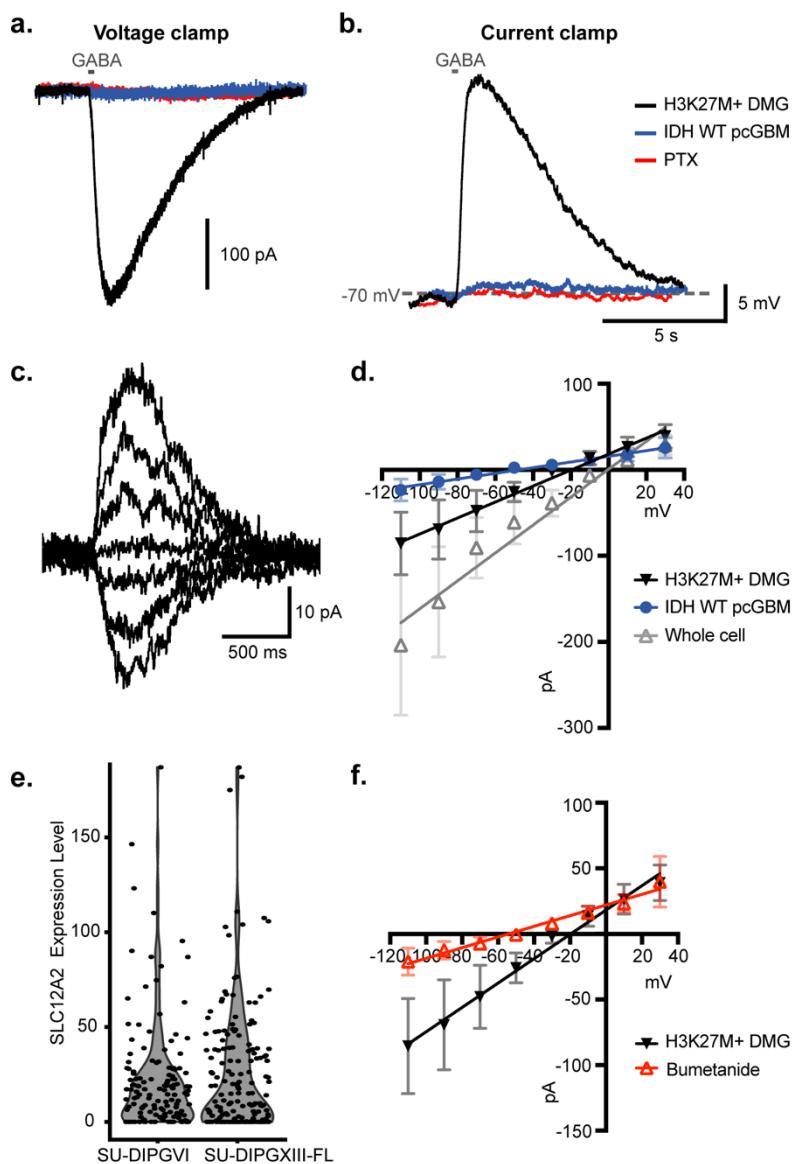
637
638 **Figure 2. GABA is depolarizing in DMG, but not IDH wild type glioblastoma.**

639 **a-b.** Perforated patch of xenografted patient-derived H3K27M+ DMG cells and

640 hemispheric (IDH/H3 WT) pediatric cortical glioblastoma (pcGBM) reveals varying current

641 sizes (in voltage clamp, **a.**) and levels of depolarization (in current clamp, **b.**) in response

642 to local GABA application.

643 **c.** Representative trace of H3K27M+ DMG cell response to GABA at varying membrane

644 potentials.

645 **d.** Current-voltage relationship of GABA current in DMG cells and IDH WT pcGBM cells

646 recorded with perforated patch and whole-cell patch clamp electrophysiology. Reversal

647 potential of GABA was -19.61 mV in H3K27M+ DMG cells (n = 6 cells from 5 mice), -

648 47.44 mV in IDH WT pcGBM cells (n = 6 cells from 5 mice), and -0.4051 mV during whole-

649 cell recording of H3K27M+ DMG cells with a high Cl⁻ internal solution (n = 4 cells from 4

650 mice).

651 **e.** Single cell RNAseq analysis of SLC12A2 (NKCC1) in patient-derived DMG xenografts.

652 **f.** Current-voltage relationship of H3K27M+ DMG cells in the presence of 100 µM

653 bumetanide, a NKCC1 inhibitor. Reversal potential of GABA in DMG cells is -54.20 mV

654 in the presence of bumetanide (n = 5 cells from 3 mice). All data are mean ± s.e.m.

655
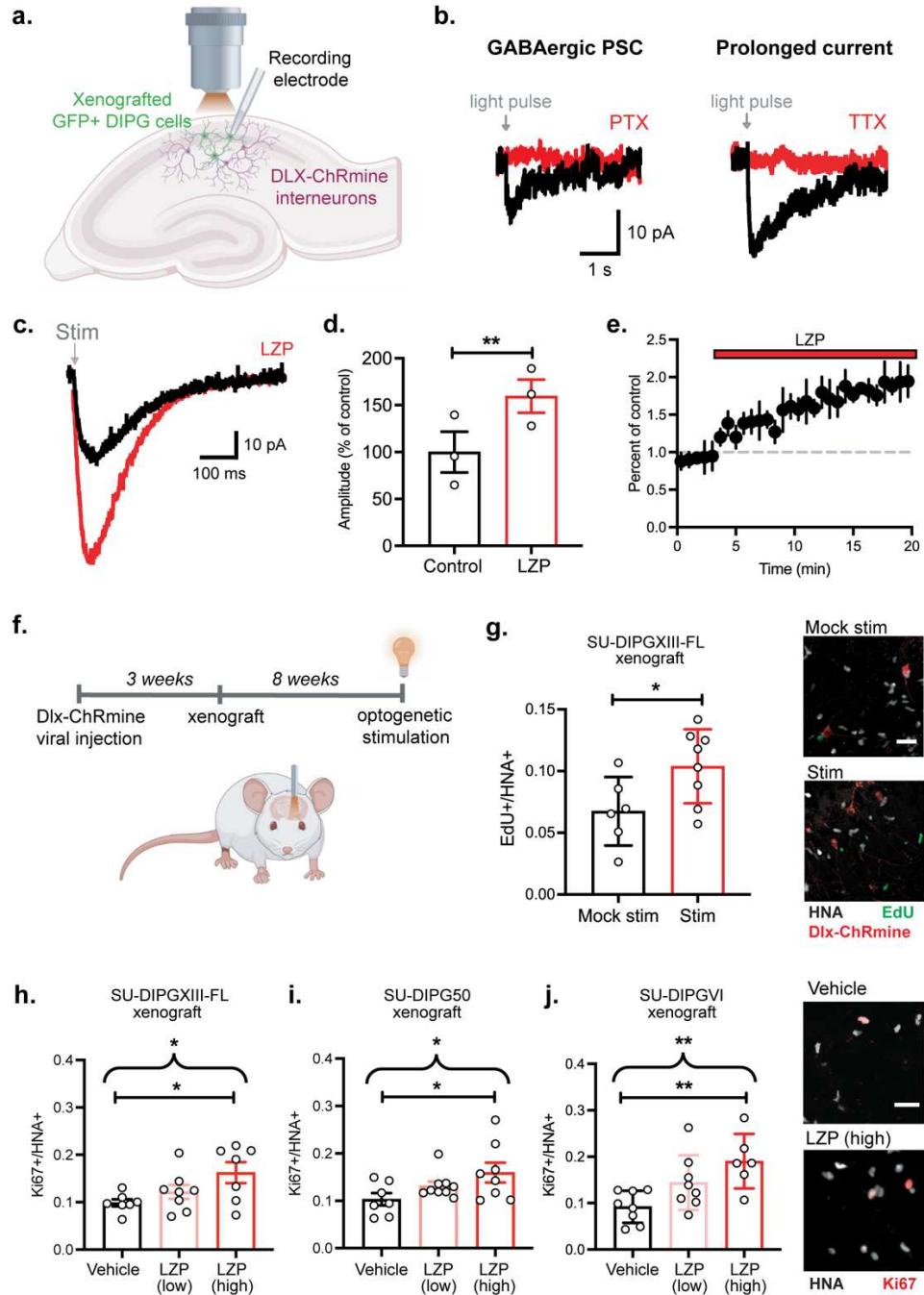
Figure 3. GABAergic interneuron activity drives DMG proliferation.

a. Patient-derived DMG cells expressing GFP were xenografted into the CA1 region of the hippocampus of NSG mice. Response to optogenetic stimulation of GABAergic

660   interneurons expressing DLX-ChRmine was recorded in xenografted cells using patch

661   clamp electrophysiology.

662   **b.** Two types of responses to optogenetic stimulation of GABAergic neurons were

663   recorded in DMG cells: a PTX-sensitive GABAergic PSC (top) and a prolonged

664   tetrodotoxin (TTX)-sensitive current (bottom).

665   **c.** Representative trace of GABAergic PSCs in DMG in the absence and presence of 10

666   μM lorazepam (LZP), a benzodiazepine.

667   **d.** Quantification of current amplitude after LZP perfusion as a % of control (n = 3 cells

668   from 3 mice), paired Student's t-test.

669   **e.** Time course of GABAergic PSC decrease in response to LZP.

670   **f.** Experimental paradigm for *in vivo* optogenetic stimulation of DLX-ChRmine

671   interneurons near xenografted DMG cells in the CA1 region of the hippocampus.

672   **g.** Quantification of proliferation index (EdU+/HNA+ cells) after optogenetic stimulation or

673   mock stimulation (left; mock stim, n = 6 mice; stim, n = 8 mice, two-tailed Student's t-test).

674   Right, representative confocal images of DLX-ChRmine GABAergic interneurons (red)

675   near xenografted DMG cells expressing EdU (green) and HNA (white). Scale bar, 25 μm.

676   **h-j.** Dose-dependent (low = 2 mg/kg; high = 8 mg/kg) effect of LZP treatment in mice with

677   patient-derived DMG xenografts, SU-DIPGXIII-FL (vehicle, n = 7 mice; low dose, n = 8

678   mice; high dose, n = 7 mice; **h**), SU-DIPG50 (vehicle, n = 7 mice; low dose, n = 9 mice;

679   high dose, n = 8 mice; **i**), and SU-DIPGVI (vehicle, n = 8 mice; low dose, n = 8 mice; high

680   dose, n = 6 mice; **j**), one-way ANOVA. Straight brackets indicate Dunnett's multiple

681   comparisons test between two groups; curved brackets indicate post-test for linear

682   contrast among all three groups. Right, representative confocal images of xenografted

683   SU-DIPGVI cells expressing Ki67 (red) and HNA (white). Scale bar, 25 μm. All data are

684   mean ± s.e.m. *P < 0.05, **P < 0.01.

685
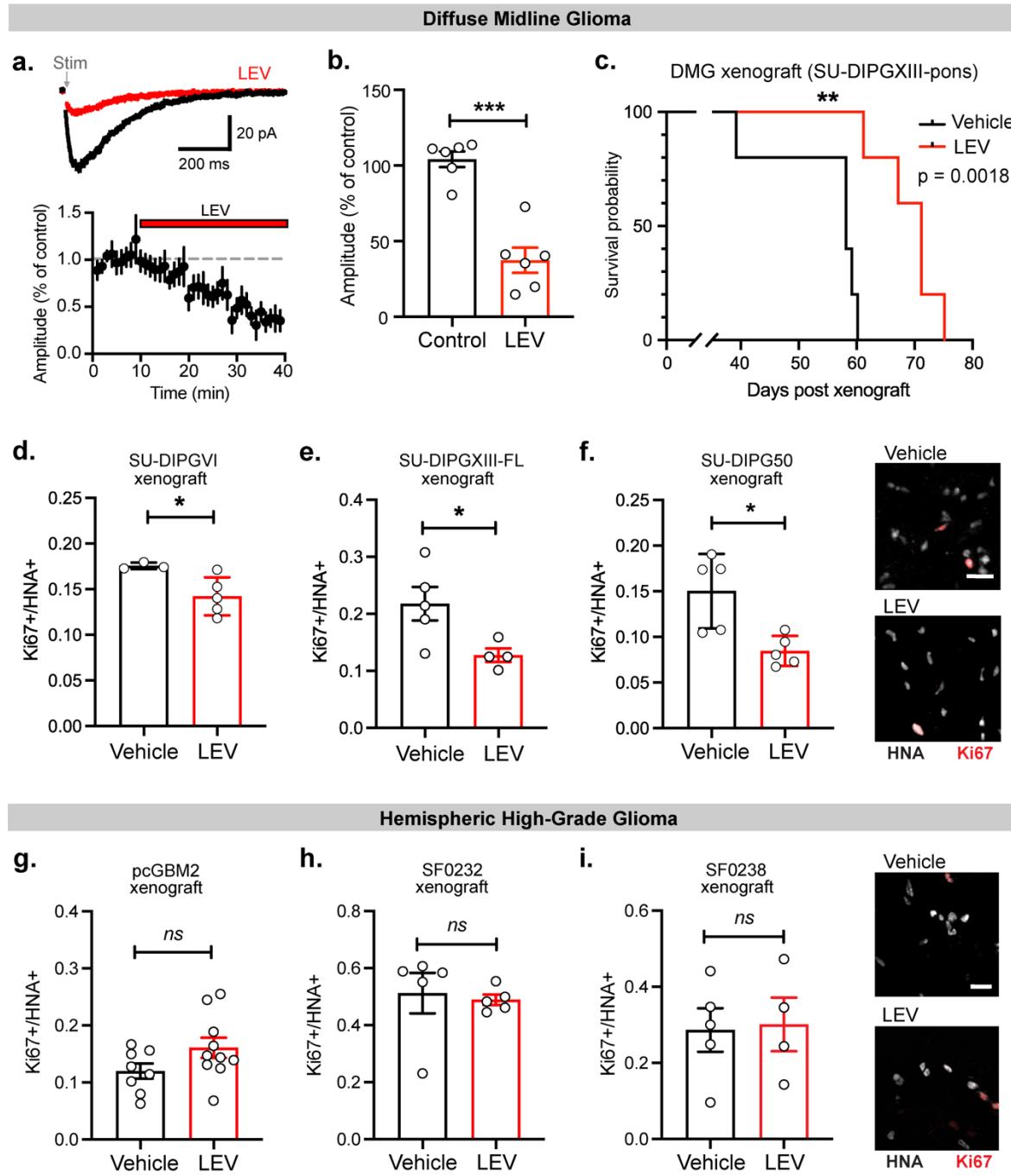
Figure 4. Targeting neuron-to-glioma synapses reduces tumor progression in DMG.

689 **a.** Representative trace of GABAergic PSCs in DMG in the absence and presence of 100

690 µM levetiracetam (LEV), an anti-epileptic drug. Below, time course of GABAergic PSC

691 decrease in response to LEV.

692 **b.** Quantification of current amplitude after LEV perfusion as a % of control (n = 6 cells

693 from 5 mice), paired Student's t-test.

694 **c.** Kaplan–Meier survival curves of mice with xenografted SU-DIPG-XIII-P tumors treated

695 with LEV or vehicle (n = 5 mice per group).

696 **d-f.** Effect of LEV treatment in mice with patient-derived DMG xenografts, SU-DIPGVI

697 (vehicle, n = 3; LEV, n = 5; **d.**), SU-DIPGXIII-FL (vehicle, n = 5 mice; LEV, n = 4 mice; **e.**),

698 and SU-DIPG50 (vehicle, n = 5 mice; LEV, n = 5 mice; **f.**), two-tailed Student's t-test.

699 Right, representative confocal images of xenografted SU-DIPG50 cells expressing Ki67

700 (red) and HNA (white). Scale bar, 25 µm.

701 **g.-i.** No effect of LEV treatment in mice with patient-derived hemispheric high-grade

702 glioma xenografts, pcGBM2 (vehicle, n = 8; LEV, n = 10; **g.**), SF0232 (vehicle, n = 5 mice;

703 LEV, n = 5 mice; **h.**) and SF0238 (vehicle, n = 5 mice; LEV, n = 4 mice), two-tailed

704 Student's t-test. Right, representative confocal images of xenografted SF0238 cells

705 expressing Ki67 (red) and HNA (white). Scale bar, 25 µm. All data are mean ± s.e.m. *P

706 < 0.05, **P < 0.01, ***P < 0.001.

707

708
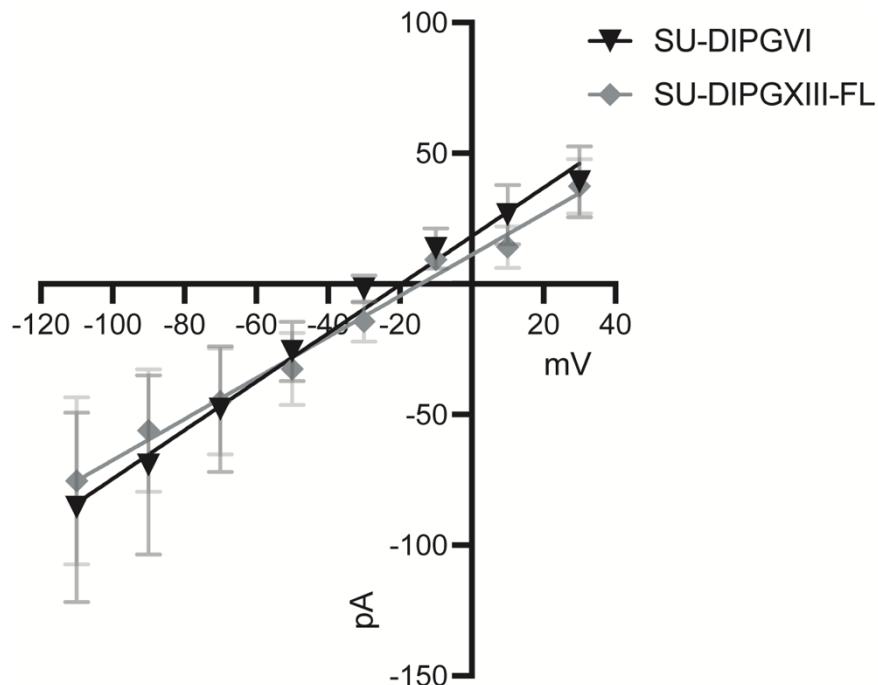
709
710
711 **Extended Data Figure 1. Current-voltage relationship of GABA current in two**

712 **patient-derived DMG xenograft models recorded with perforated patch.** Reversal

713 potential of GABA was -19.61 mV in SU-DIPGVI cells (n = 6 cells from 5 mice), and -

714 14.14 mV in SU-DIPGXIII-FL cells (n=5 cells from 3 mice). All data are mean ± s.e.m.
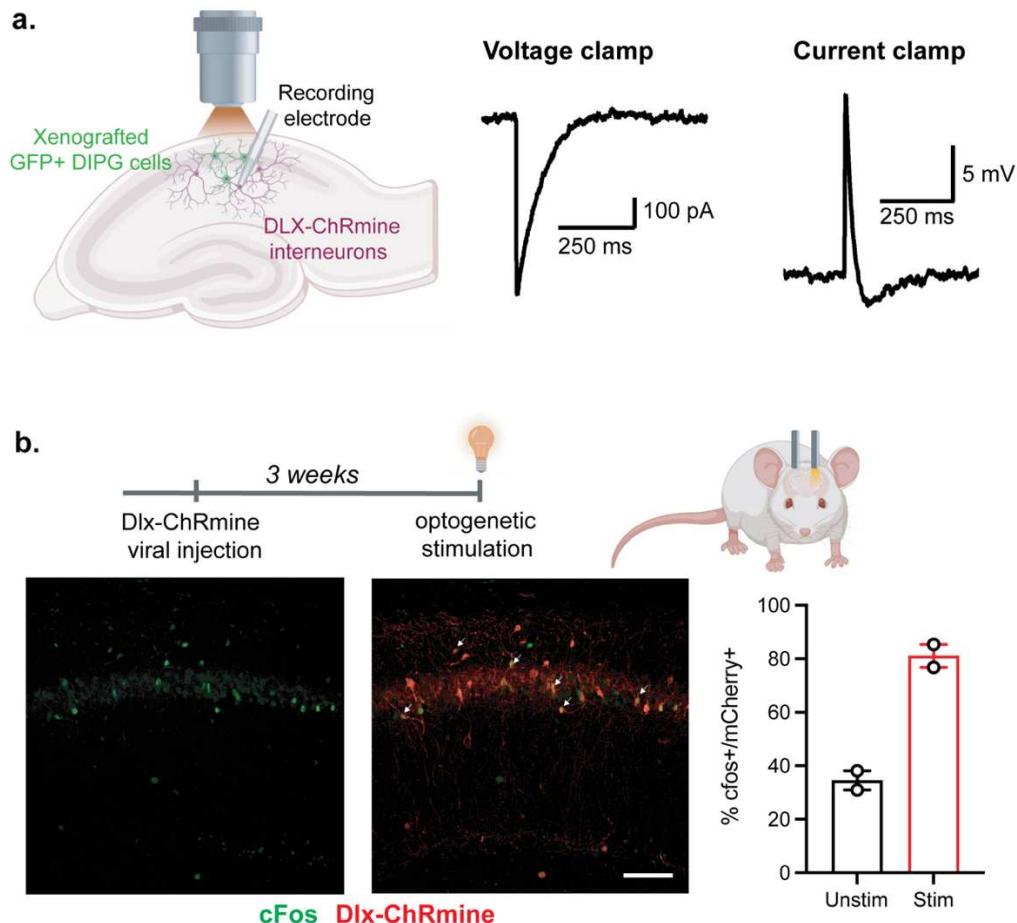
Extended Data Figure 2. Optogenetic stimulation of GABAergic interneurons expressing DLX-ChRmine.

a. Inward current and corresponding depolarization of GABAergic interneurons expressing DLX-ChRmine in response to optogenetic stimulation were recorded in using patch clamp electrophysiology.

b. Optogenetic stimulation of interneurons expressing DLX-ChRmine (red) lead to neuronal activity, indicated by cfos expression (green). Arrows indicate co-labeled cells. Scale bar, 100 µm. Above, experimental timeline. Right, quantification of cfos expression in interneurons in the stimulated hemisphere (stim) is greater than in the unstimulated hemisphere (unstim, n = 2 mice). All data are mean ± s.e.m.
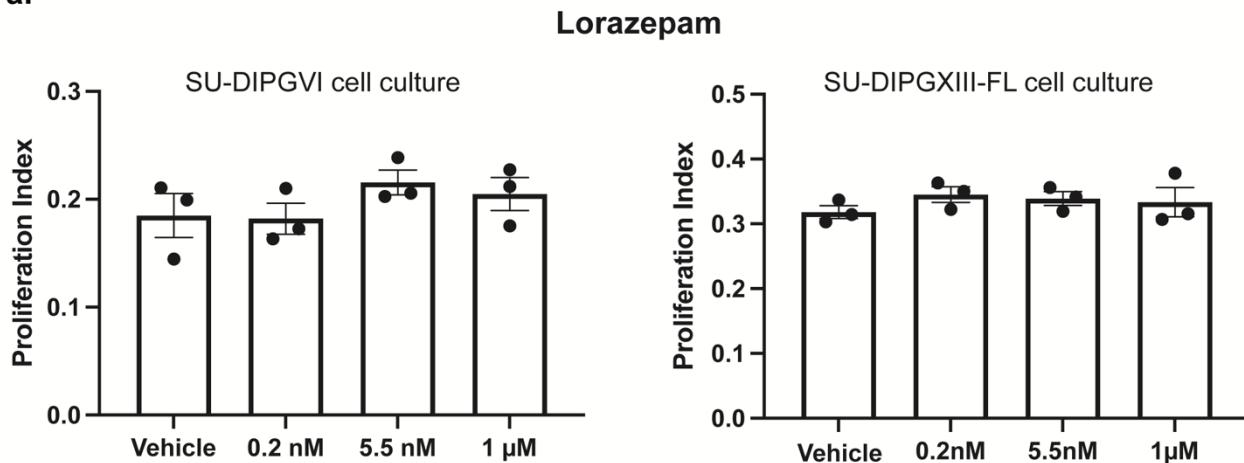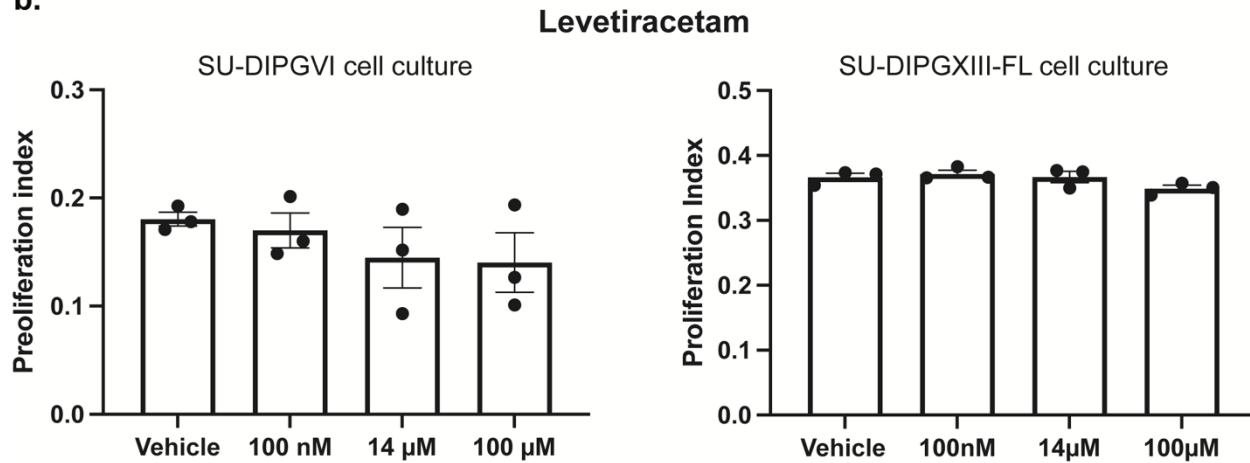
Extended Data Figure 3. Lorazepam and levetiracetam have no effect on proliferation of patient-derived DMG cells in monoculture

a. Lorazepam treatment in patient-derived DMG cultures SU-DIPGVI and SU-DIPGXIII-FL had no effect on proliferation (n = 3 wells per group).

b. Levetiracetam treatment in patient-derived DMG cultures SU-DIPGVI and SU-DIPGXIII-FL had no effect on proliferation (n = 3 wells per group). All data are mean ± s.e.m. Two-tailed Student's t-test.
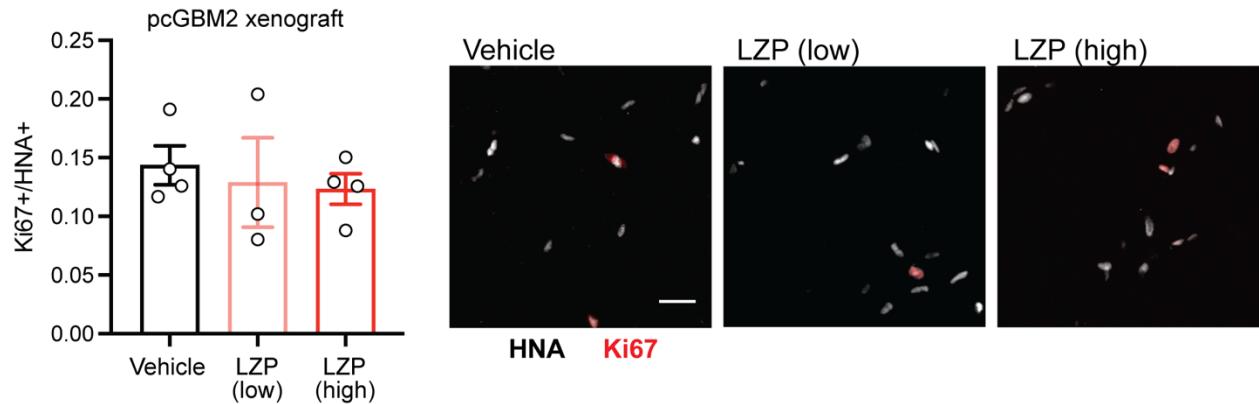
Extended Data Figure 4. Lorazepam has no effect on H3/IDH WT pediatric GBM. LZP treatment in mice with patient-derived pcGBM2 xenografts has no effect on cell proliferation (vehicle, n = 4 mice; low dose, n = 3 mice; high dose, n = 4 mice). Representative confocal images of xenografted pcGBM2 cells expressing Ki67 (red) and HNA (white; right). Scale bar, 25 µm. All data are mean ± s.e.m. One-way ANOVA.
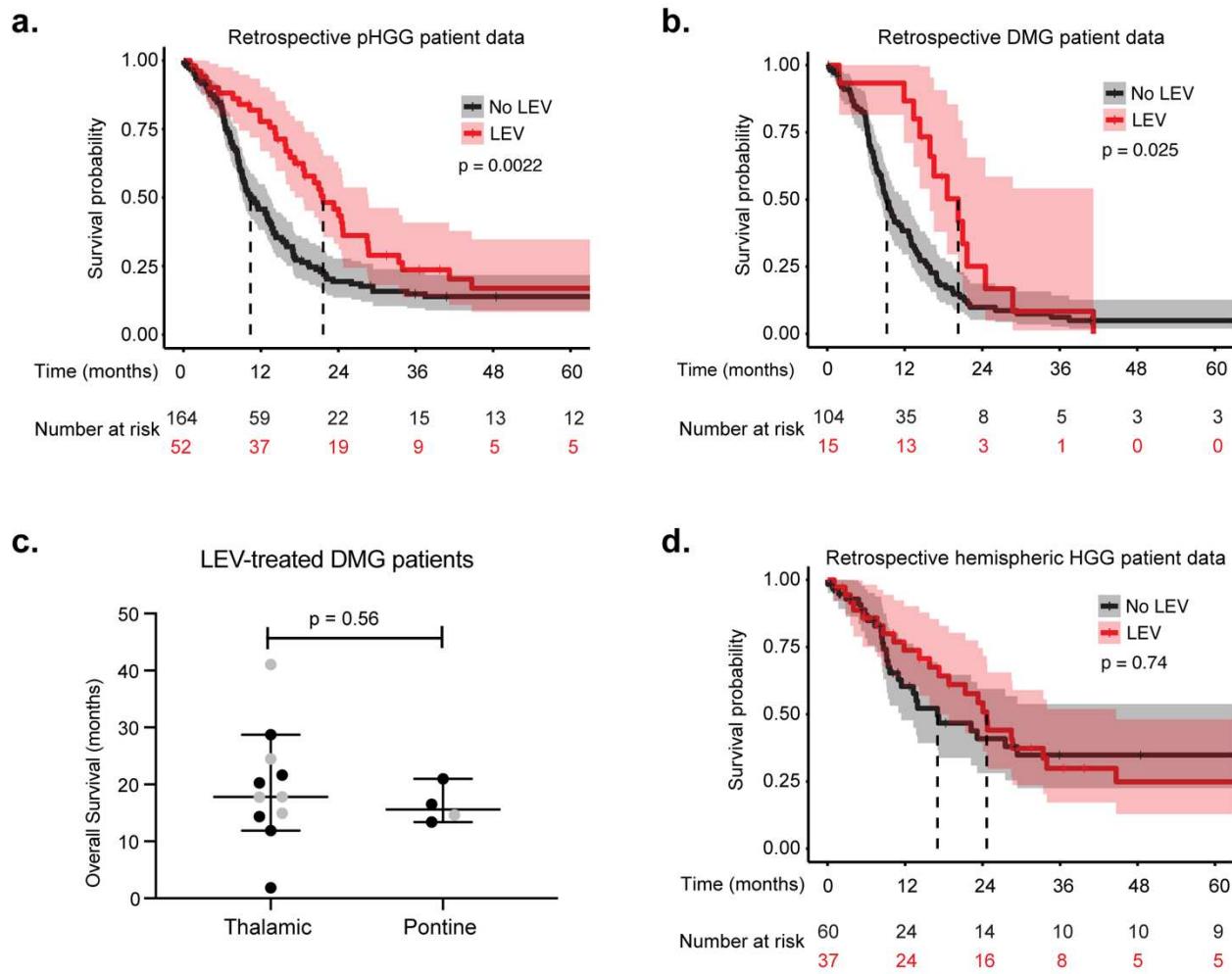
Extended Data Figure 5. Effect of levetiracetam on overall survival in retrospective, real-world patient data.

a. All pediatric high-grade gliomas: Kaplan–Meier overall survival (OS) curves of retrospective data from Stanford University (1990-2020) and University of Michigan (2012-2021) patient databases (n=216), showing pediatric high-grade glioma (pHGG) patients treated with LEV (LEV: median OS = 21.7 months, n = 52; no LEV: median OS= 10.4 months, n = 164).

b. Diffuse midline gliomas: Kaplan–Meier overall survival (OS) curves of retrospective data from DMG patients treated with LEV (LEV: median OS = 20.3 months, n = 15; no LEV: median OS= 9.2 months, n = 105).

756   **c.** No difference in overall survival of LEV-treated patients with thalamic compared to

757   pontine DMG (thalamic: n = 11; pontine: n = 4). Grey points are data censored at time of

758   last follow-up. Data are median ± 95% CI. n.s. (P>0.05), two-tailed Student's t-test.

759   **d.** Hemispheric high-grade gliomas: Kaplan–Meier overall survival (OS) curves of

760   retrospective data from hemispheric high-grade glioma (HGG) patients treated with LEV

761   (LEV: OS=24.6 months, n = 37; no LEV: OS = 17.0 months, n = 60).

762
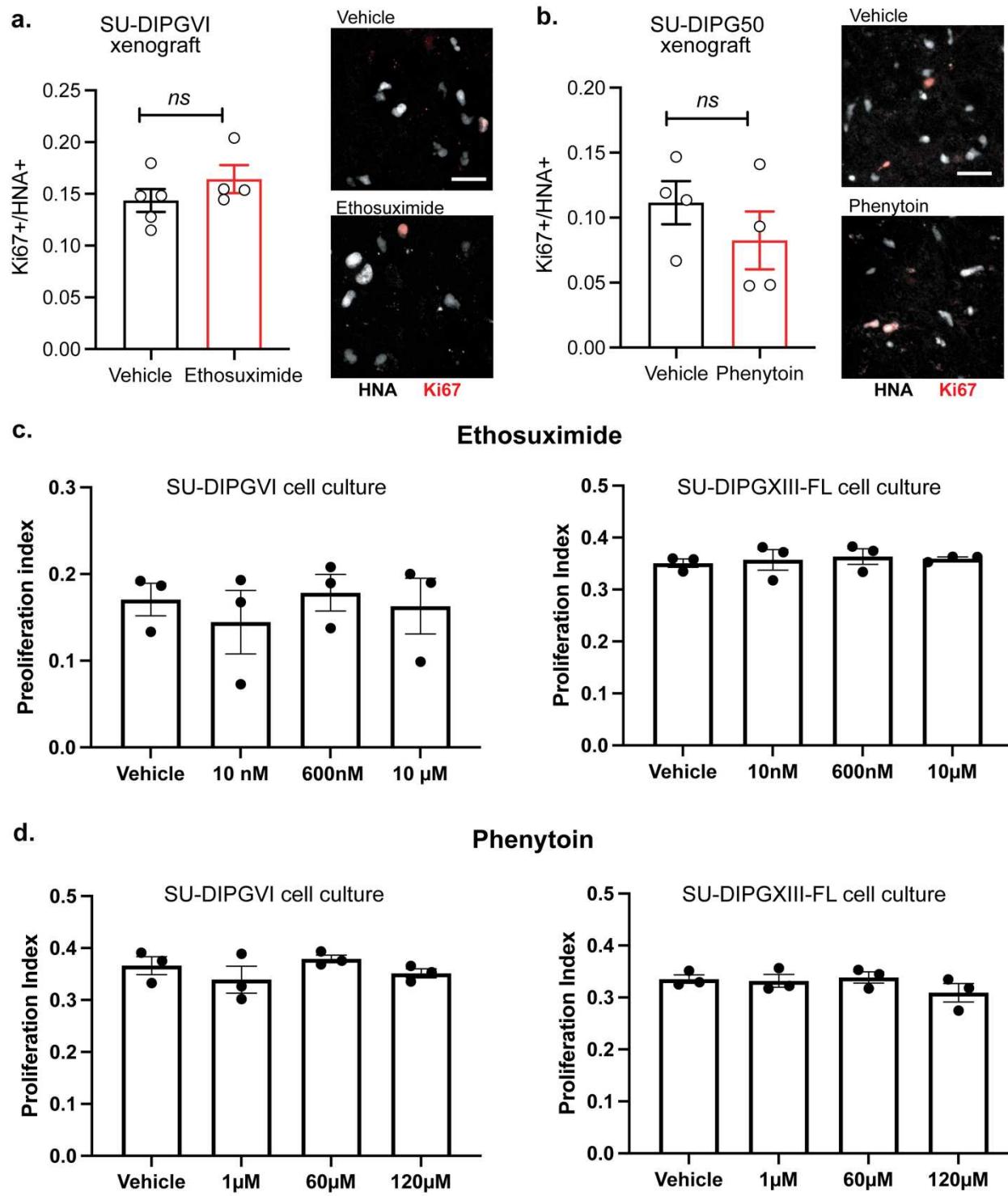
Extended Data Figure 6. Antiepileptic drugs ethosuximide and phenytoin do not affect DMG proliferation.

766 **a.** Ethosuximide treatment in mice with patient-derived SU-DIPGVI xenografts has no

767 effect on cell proliferation (vehicle, n = 5 mice; ethosuximide, n = 4 mice). Representative

768 confocal images of xenografted SU-DIPGVI cells expressing Ki67 (red) and HNA (white;

769 right). Scale bar, 25 µm.

770 **b.** Phenytoin treatment in mice with patient-derived SU-DIPG50 xenografts has no effect

771 on cell proliferation (vehicle, n = 4 mice; phenytoin, n = 4 mice). Representative confocal

772 images of xenografted SU-DIPG50 cells expressing Ki67 (red) and HNA (white; right).

773 Scale bar, 25 µm.

774 **c.** Ethosuximide treatment in patient-derived DMG cultures SU-DIPGVI and SU-DIPGXIII-

775 FL had no effect on proliferation (n = 3 wells per group).

776 **d.** Phenytoin treatment in patient-derived DMG cultures SU-DIPGVI and SU-DIPGXIII-FL

777 had no effect on proliferation (n = 3 wells per group). All data are mean ± s.e.m. Two-

778 tailed Student's t-test.

779
780
781 Literature Cited
782
783 1 Venkatesh, H. S. *et al.* Neuronal Activity Promotes Glioma Growth through Neuroligin-3
784 Secretion. *Cell* **161**, 803-816 (2015). https://doi.org:10.1016/j.cell.2015.04.012
785 2 Pan, Y. *et al.* NF1 mutation drives neuronal activity-dependent initiation of optic glioma.
786 *Nature* **594**, 277-282 (2021). https://doi.org:10.1038/s41586-021-03580-6
787 3 Venkatesh, H. S. *et al.* Electrical and synaptic integration of glioma into neural circuits.
788 *Nature* **573**, 539-545 (2019). https://doi.org:10.1038/s41586-019-1563-y
789 4 Venkataramani, V. *et al.* Glutamatergic synaptic input to glioma cells drives brain tumour
790 progression. *Nature* **573**, 532-538 (2019). https://doi.org:10.1038/s41586-019-1564-x
791 5 Venkataramani, V. T. K., Frank Winkler. Glioblastoma hijacks neuronal mechanisms for
792 brain invasion. *Cell* **in press** (2022).
793 6 Mackay, A. *et al.* Integrated Molecular Meta-Analysis of 1,000 Pediatric High-Grade and
794 Diffuse Intrinsic Pontine Glioma. *Cancer Cell* **32**, 520-537 e525 (2017).
795 https://doi.org:10.1016/j.ccell.2017.08.017
796 7 Cooney, T. *et al.* Contemporary survival endpoints: an International Diffuse Intrinsic
797 Pontine Glioma Registry study. *Neuro Oncol* **19**, 1279-1280 (2017).
798 https://doi.org:10.1093/neuonc/nox107

799   8   Schwartzentruber, J. *et al.* Driver mutations in histone H3.3 and chromatin remodelling
800   genes   in   paediatric   glioblastoma.   *Nature*   **482**,   226-231   (2012).
801   https://doi.org:10.1038/nature10833
802   9   Wu, G. *et al.* Somatic histone H3 alterations in pediatric diffuse intrinsic pontine gliomas
803   and   non-brainstem   glioblastomas.   *Nat   Genet*   **44**,   251-253   (2012).
804   https://doi.org:10.1038/ng.1102
805   ng.1102 [pii]
806   10   Khuong-Quang, D. A. *et al.* K27M mutation in histone H3.3 defines clinically and
807   biologically distinct subgroups of pediatric diffuse intrinsic pontine gliomas. *Acta
808   Neuropathol* **124**, 439-447 (2012). https://doi.org:10.1007/s00401-012-0998-0
809   11   Monje, M. *et al.* Hedgehog-responsive candidate cell of origin for diffuse intrinsic pontine
810   glioma. *Proc Natl Acad Sci U S A* **108**, 4453-4458 (2011). https://doi.org:1101657108 [pii]
811   10.1073/pnas.1101657108
812   12   Nagaraja, S. *et al.* Transcriptional Dependencies in Diffuse Intrinsic Pontine Glioma.
813   *Cancer Cell* **31**, 635-652 e636 (2017). https://doi.org:10.1016/j.ccell.2017.03.011
814   13   Filbin, M. G. *et al.* Developmental and oncogenic programs in H3K27M gliomas dissected
815   by   single-cell   RNA-seq.   *Science*   **360**,   331-335   (2018).
816   https://doi.org:10.1126/science.aao4750
817   14   Nagaraja, S. *et al.* Histone Variant and Cell Context Determine H3K27M Reprogramming
818   of the Enhancer Landscape and Oncogenic State. *Molecular cell* **76**, 965-980 e912 (2019).
819   https://doi.org:10.1016/j.molcel.2019.08.030
820   15   Haag, D. *et al.* H3.3-K27M drives neural stem cell-specific gliomagenesis in a human
821   iPSC-derived   model.   *Cancer   Cell*   **39**,   407-422   e413   (2021).
822   https://doi.org:10.1016/j.ccell.2021.01.005
823   16   Geraghty, A. C. *et al.* Loss of Adaptive Myelination Contributes to Methotrexate
824   Chemotherapy-Related Cognitive Impairment. *Neuron* **103**, 250-265 e258 (2019).
825   https://doi.org:10.1016/j.neuron.2019.04.032
826   17   Makinodan, M., Rosen, K., Ito, S. & Corfas, G. A critical period for social experience-
827   dependent oligodendrocyte maturation and myelination. *Science* **337**, 1357-1360 (2012).
828   https://doi.org:10.1126/science.1220845
829   18   Swire, M., Kotelevtsev, Y., Webb, D. J., Lyons, D. A. & Ffrench-Constant, C. Endothelin
830   signalling mediates experience-dependent myelination in the CNS. *Elife* **8** (2019).
831   https://doi.org:10.7554/eLife.49493
832   19   Bergles, D. E., Roberts, J. D., Somogyi, P. & Jahr, C. E. Glutamatergic synapses on
833   oligodendrocyte precursor cells in the hippocampus. *Nature* **405**, 187-191 (2000).
834   https://doi.org:10.1038/35012083
835   20   Lin, S. C. & Bergles, D. E. Synaptic signaling between GABAergic interneurons and
836   oligodendrocyte precursor cells in the hippocampus. *Nat Neurosci* **7**, 24-32 (2004).
837   https://doi.org:10.1038/nn1162
838   21   Mount, C. W., Yalcin, B., Cunliffe-Koehler, K., Sundaresh, S. & Monje, M. Monosynaptic
839   tracing maps brain-wide afferent oligodendrocyte precursor cell connectivity. *Elife* **8**
840   (2019). https://doi.org:10.7554/eLife.49291
841   22   Karadottir, R., Cavelier, P., Bergersen, L. & Attwell, D. NMDA receptors are expressed in
842   oligodendrocytes   and   activated   in   ischaemia.   *Nature*   **438**,   1162-1166   (2005).
843   https://doi.org:10.1038/nature04302

844   23   Kukley, M. *et al.* Glial cells are born with synapses. *FASEB journal : official publication*
845   *of the Federation of American Societies for Experimental Biology* **22**, 2957-2969 (2008).
846   https://doi.org:10.1096/fj.07-090985

847   24   Gibson, E. M. *et al.* Neuronal activity promotes oligodendrogenesis and adaptive
848   myelination in the mammalian brain. *Science* **344**, 1252304 (2014).
849   https://doi.org:10.1126/science.1252304

850   25   Venkatesh, H. S. *et al.* Targeting neuronal activity-regulated neuroligin-3 dependency in
851   high-grade glioma. *Nature* **549**, 533-537 (2017). https://doi.org:10.1038/nature24014

852   26   Chen, P. *et al.* Olfactory sensory experience regulates gliomagenesis via neuronal IGF1.
853   *Nature* (2022). https://doi.org:10.1038/s41586-022-04719-9

854   27   Rivera, C. *et al.* The K+/Cl- co-transporter KCC2 renders GABA hyperpolarizing during
855   neuronal maturation. *Nature* **397**, 251-255 (1999). https://doi.org:10.1038/16697

856   28   Marshel, J. H. *et al.* Cortical layer-specific critical dynamics triggering perception. *Science*
857   **365** (2019). https://doi.org:10.1126/science.aaw5202

858   29   Robison, N. J. & Kieran, M. W. Diffuse intrinsic pontine glioma: a reassessment. *J*
859   *Neurooncol* **119**, 7-15 (2014). https://doi.org:10.1007/s11060-014-1448-8

860   30   Taylor, K. R. *et al.* Glioma synapses recruit mechanisms of adaptive plasticity. *bioRxiv*,
861   2021.2011.2004.467325 (2021). https://doi.org:10.1101/2021.11.04.467325

862   31   Labrakakis, C., Patt, S., Hartmann, J. & Kettenmann, H. Functional GABA(A) receptors
863   on human glioma cells. *Eur J Neurosci* **10**, 231-238 (1998).

864   32   Pallud, J. *et al.* Effect of Levetiracetam Use Duration on Overall Survival of Isocitrate
865   Dehydrogenase Wild-Type Glioblastoma in Adults: An Observational Study. *Neurology*
866   **98**, e125-e140 (2022). https://doi.org:10.1212/WNL.0000000000013005

867   33   Happold, C. *et al.* Does Valproic Acid or Levetiracetam Improve Survival in
868   Glioblastoma? A Pooled Analysis of Prospective Clinical Trials in Newly Diagnosed
869   Glioblastoma. *J Clin Oncol* **34**, 731-739 (2016).
870   https://doi.org:10.1200/JCO.2015.63.6563

871   34   Chen, J. S. *et al.* The effect of levetiracetam treatment on survival in patients with
872   glioblastoma: a systematic review and meta-analysis. *J Neurooncol* **156**, 257-267 (2022).
873   https://doi.org:10.1007/s11060-021-03940-2

874   35   Blanchart, A. *et al.* Endogenous GABAA receptor activity suppresses glioma growth.
875   *Oncogene* **36**, 777-786 (2017). https://doi.org:10.1038/onc.2016.245

876   36   Tantillo, E. *et al.* Differential roles of pyramidal and fast-spiking, GABAergic neurons in
877   the control of glioma cell proliferation. *Neurobiol Dis* **141**, 104942 (2020).
878   https://doi.org:10.1016/j.nbd.2020.104942

879   37   Qin, E. Y. *et al.* Neural Precursor-Derived Pleiotrophin Mediates Subventricular Zone
880   Invasion by Glioma. *Cell* **170**, 845-859 e819 (2017).
881   https://doi.org:10.1016/j.cell.2017.07.016

882   38   Venteicher, A. S. *et al.* Decoupling genetics, lineages, and microenvironment in IDH-
883   mutant gliomas by single-cell RNA-seq. *Science* **355** (2017).
884   https://doi.org:10.1126/science.aai8478

885

Extended Data Table 1. Diffuse Midline Glioma Patients

Institution	Age (years)	Sex	Diagnosis	Other treatments	Levetiracetam yes/no	Overall survival (days)
University of Michigan	7	Male	Pontine diffuse midline glioma, H3.3K27M, ATRX Q119*, PPM1D G463fs, PDGFRA amplification, KIT, KDR	XRT	Yes	638
University of Michigan	12	Male	Thalamic diffuse midline glioma, H3.3K27M, TP53 H179N, ATRX R2197C, TRIO I780fs deletion, subclonal WAS exon 8 loss, Focal amplifications: HGF, MET, GAB2, TBCD Copy gain NTRK2 (4 copies)	XRT, TMZ, lomustine, Cabozantinib, subtotal resection	Yes	362
University of Michigan	9	Female	Thalamic diffuse midline glioma, H3.1K27M, EGFR A289V, MAX R60Q, PIK3CA R88Q, ARHGAP35 G854E, Subclonal: CEBPZ D78N, DIS3 I779F, MSH3 P64A, BCORL1 K1421fs deletion; subclonal E2F7 L6fs deletion; Copy gain: Chr1q, 2, 5, 7, 15p; UPD: Chr12	XRT, TMZ, Vimpat, ONC201	Yes	659
University of Michigan	13	Female	Thalamic diffuse midline glioma H3K27M, BRAF V600E	XRT, TMZ, Dabrafenib, trametinib, Bevacuzimab, Irinotecan, ONC201, subtotal resection	Yes	Censored at 745
University of Michigan	8	Male	Thalamic diffuse midline glioma, BRAF V600E, H3WT	XRT, Dabrafenib, trametinib, Trileptal, gabapentin, Vimpat	Yes	Censored at 540
University of Michigan	13	Male	Thalamic diffuse midline glioma	XRT, TMZ, ONC201, Oxcarbazine, Zonisamide	Yes	617
University of Michigan	20	Male	Pontine diffuse midline glioma, H3K27M mutant	XRT, TMZ, Depakote, ONC201	Yes	Censored at 446
University of Michigan	10	Female	Thalamic diffuse midline, FBXW R465H, STAG2 R110, SETD2 R2165, VAV1 657A, FGFR3 copy gain, CDK11A/B homozygous deletion, gene fusion FGFR3-PHGDH, FGFR3 copy gain, Gain: chromosomes 1q and 7q; Loss: chromosomes 1p, 4p15-16, 6q, and 10q, H3WT	XRT, COG clinical trial ACNS0831, ponatinib	Yes	Censored at 1249

University of Michigan	10	Male	Thalamic diffuse midline glioma, H3K27M mutation; two TP53 mutations, IDH-1 negative, no MGMT methylation	XRT, ONC201, Bevacizumab, Vimpat, subtotal resection	Yes	Censored at 542
University of Michigan	12	Male	Thalamic diffuse midline glioma, H3K27M mutation; ATRX pR1803H, recurrent (ChrX), NTRK2 internal tandem duplication, focal amplification	XRT, TMZ, ONC201, bevacizumab, entrectinib, subtotal resection	Yes	Censored at 454
Stanford University	6	Female	Pontine diffuse midline glioma	XRT, Etoposide	Yes	407
Stanford University	2	Female	Pontine diffuse midline glioma	XRT	Yes	503
Stanford University	11	Female	Thalamic diffuse midline glioma, H3WT, IDH1/2 WT, ATRX and TP53 mutated	XRT, TMZ, Lomustine, Savolitinib	Yes	874
Stanford University	13	Female	Thalamic diffuse midline glioma, H3K27-altered	NA	Yes	56
Stanford University	11	Male	Thalamic diffuse midline glioma	XRT, TMZ, etoposide	Yes	436
University of Michigan	17	Male	Pontine/spinal diffuse midline glioma, H3.3 K27M, TP53 H179R, ATRX D1313fs, ERCC5 K917fs, Homozygous loss: NF1 Copy loss: BRCA1, CDK12	XRT, SAHA (HDAC inhibitor), subtotal resection	No	316
University of Michigan	5	Female	Pontine diffuse midline glioma, PIK3CA; H3.1 K27M	XRT, everolimus, bevacuzimab, panobinostat, subtotal resection	No	Censored at 588
University of Michigan	13	Male	Pontine diffuse midline glioma, H3.3K27M mutation; FGFR3 activating mutation, loss of BCOR	XRT, bevacizumab, ponatinib, Panobinostat, pazopanib, everolimus subtotal resection	No	Censored at 533
University of Michigan	12	Male	Thalamic diffuse midline glioma, somatic mutations in EGFR V292L, mutation/loss in CDKN2C and BCOR1, EGFR T483_G485del, gene fusion ELF4-SMARCA1, H3WT	Proton XRT, TPCV, Osimertinib, bevacizumab	No	Censored 502
University of Michigan	8	Male	Pontine diffuse midline glioma, H3.3K27M	XRT, COG phase 1 trial (ADVL1217), everolimus, panobinostat, Depakote	No	Censored at 259
University of Michigan	2	Male	Pontine diffuse midline glioma, H3.3K27M, TP53 R273C, CTTNBP2-MET, in frame with MET kinase domain	XRT, cabozantinib	No	Censored at 246

Institution	Age	Sex	Diagnosis	Treatment		Outcome
University of Michigan	9	Female	Pontine diffuse midline glioma, H3.3K27M, PPM1D E525, TP53 R248W, additional non-recurrent missense mutations: AFF2 T385N, ABCC1 T826M, PIK3C2G S1183R, PTPRJ E841fs; Copy gain: Chr 1q, 8q, 17q; Loss of Chr11q	Proton XRT, XRT, ONC201	No	
University of Michigan	1	Female	Pontine/thalamic diffuse midline glioma, H3K27M	NA	No	Censored at 29
University of Michigan	7	Female	Pontine diffuse midline glioma, H3.1 K27M, ACVR1 R206H, USP9X splice acceptor, exon33, BCOR A603fs deletion	XRT, ONC201 (arm a), bevacizumab	No	Censored at 626
University of Michigan	13	Male	Thoracic spine diffuse midline glioma, H3.3 K27M, ATRX mutation, FGFR1, H3.3 G34W, PPM1D, PTPN11	XRT, ONC201, bevacizumab, subtotal resection	No	Censored at 398
University of Michigan	17	Female	Thalamic diffuse midline glioma, H3.3, ATRX, PI3KR1, TP53 mutations	Proton XRT, PTC56, ONC201, Subtotal resection	No	Censored at 216
University of Michigan	2	Female	Thalamic diffuse midline glioma, H3K27M	Proton XRT, ONC201	No	Censored at 176
University of Michigan	9	Female	Pontine diffuse midline glioma, H3.3K27M, PDGFA A153T, TP53 P222_E224delinL, IGF1R focal amplification	Proton XRT, ONC201, bevacizumab	No	Censored at 459
University of Michigan	9	Male	Tectal/thalamic diffuse midline glioma, H3K27M mutation, KRAS 212R mutation, HGF amplification	Proton XRT, vincristine, carboplatin, trametinib, ONC201, Subtotal resection	No	Censored at 2220
Stanford University	6	Female	Pontine diffuse midline glioma	XRT, Cisplatin	No	182
Stanford University	16	Male	Pontine diffuse midline glioma	XRT	No	7
Stanford University	5	Male	Pontine diffuse midline glioma	XRT, TMZ, Vorinostat	No	424
Stanford University	7	Male	Pontine diffuse midline glioma	XRT, TMZ	No	50
Stanford University	7	Female	Pontine diffuse midline glioma	XRT, TMZ, Valproic Acid	No	416
Stanford University	15	Male	Pontine diffuse midline glioma	XRT	No	125
Stanford University	9	Male	Pontine diffuse midline glioma	XRT	No	180

Stanford University	13	Male	Pontine diffuse midline glioma, H3.1K27M, MAPKAPK2 gain	XRT, Arsenic Trioxide	No	625
Stanford University	5	Male	Pontine diffuse midline glioma	XRT	No	58
Stanford University	7	Female	Thalamic diffuse midline glioma	XRT, TMZ, Arsenic Trioxide, Bevacizumab, Carmustine, Eroltinib, Irinotecan, Sirolimus, diazepam, phenobarbital, Subtotal Resection	No	1055
Stanford University	9	Female	Pontine diffuse midline glioma	XRT, TMZ	No	231
Stanford University	5	Female	Pontine diffuse midline glioma	XRT	No	110
Stanford University	4	Female	Pontine diffuse midline glioma	XRT, nivolumab	No	Censored at 8
Stanford University	10	Female	Thalamic diffuse midline glioma, H3K27-altered	XRT, TMZ	No	Censored at 1241
Stanford University	4	Female	Pontine diffuse midline glioma	NA	No	116
Stanford University	3	Male	Pontine diffuse midline glioma	NA	No	437
Stanford University	9	Male	Medulla diffuse midline glioma	XRT, TMZ, Bevacizumab, Imetelstat, Carmustine, Subtotal Resection	No	2938
Stanford University	3	Female	Pontine diffuse midline glioma	NA	No	35
Stanford University	8	Female	Pontine diffuse midline glioma	XRT	No	Censored at 53
Stanford University	8	Female	Pontine diffuse midline glioma	XRT	No	281
Stanford University	8	Male	Pontine diffuse midline glioma	XRT	No	197
Stanford University	17	Male	Ponto-medulla diffuse midline glioma	XRT, TMZ, Bevacizumab	No	2324
Stanford University	6	Female	Pontine diffuse midline glioma, H3.3K27M, HIST1H3B gain	XRT	No	54
Stanford University	6	Female	Pontine diffuse midline glioma	NA	No	13
Stanford University	4	Male	Pontine diffuse midline glioma	NA	No	141

Stanford University	6	Male	Pontine diffuse midline glioma	XRT	No	106
Stanford University	4	Male	Pontine diffuse midline glioma	XRT, Arsenic Trioxide	No	205
Stanford University	4	Male	Pontine diffuse midline glioma	XRT	No	397
Stanford University	7	Male	Pontine diffuse astrocytoma (WHO III)	NA	No	58
Stanford University	2	Female	Pontine diffuse midline glioma	NA	No	1140
Stanford University	3	Male	Pontine diffuse midline glioma	XRT	No	487
Stanford University	4	Male	Pontine diffuse midline glioma	XRT	No	196
Stanford University	6	Female	Pontine diffuse midline glioma	XRT	No	223
Stanford University	11	Female	Pontine diffuse midline glioma	XRT, Vorinostat	No	Censored at 201
Stanford University	7	Female	Pontine diffuse midline glioma	XRT	No	Censored at 5
Stanford University	10	Male	Pontine diffuse midline glioma, H3WT	XRT (only 4 doses)	No	66
Stanford University	3	Male	Pontine diffuse midline glioma, H3.1K27M, H3F3A gain, MDM4 gain, ACVR1 point mutation, NTRK1 gain, CDK18 gain, CLK1 gain, CLK2 gain, CLK4 point mutation, NUAK2 gain, STK36 gain, PPP1CB gain, MAPKAPK2 gain	XRT, Rindopepimut, GM-CSF	No	471
Stanford University	11	Male	Pontine diffuse midline glioma	XRT, TMZ, Veliparib	No	484
Stanford University	13	Female	Medulla diffuse midline glioma	XRT, TMZ, Rindopepimut, GM-CSF, imetelstat	No	245
Stanford University	6	Female	Pontine diffuse midline glioma	XRT, TMZ, Rindopepimut, GM-CSF	No	290
Stanford University	8	Male	Cervical glioblastoma (glioblastoma multiforme, astrocytoma WHO IV)	XRT, TMZ, Subtotal Resection	No	894
Stanford University	3	Male	Pontine diffuse midline glioma	XRT	No	Censored at 105
Stanford University	12	Female	Pontine diffuse midline glioma	XRT	No	195

Stanford University	8	Male	Pontine diffuse midline glioma	XRT, Bevacizumab, Imetelstat	No	384
Stanford University	8	Female	Pontine diffuse midline glioma	XRT, cabazitaxel	No	277
Stanford University	9	Female	Pontine diffuse midline glioma, H3K27-altered	NA	No	78
Stanford University	2	Male	Pontine diffuse midline glioma	XRT, cabazitaxel	No	558
Stanford University	4	Female	Pontine diffuse midline glioma, H3K27-altered	XRT, TMZ, Bevacizumab	No	Censored at 645
Stanford University	10	Female	Pontine diffuse midline glioma	XRT, TMZ, ABT-888	Yes (1 dose)	235
Stanford University	5	Male	Pontine diffuse midline glioma	XRT, TMZ, ABT-888	No	183
Stanford University	6	Male	Pontine diffuse midline glioma	XRT,nivolumab x4 doses	No	Censored at 21
Stanford University	6	Female	Pontine diffuse midline glioma, H3K27-altered	XRT, Subtotal resection, antineoplaston	No	515
Stanford University	2	Male	Pontine diffuse midline glioma	XRT, Bevacizumab	No	Censored at 25
Stanford University	14	Female	Spinal diffuse midline glioma, H3K27-altered	Subtotal Resection, XRT, TMZ, intrathecal liposomal cytarabine, panobinostat	No	198
Stanford University	13	Female	Pontine diffuse midline glioma	XRT, panobinostat	No	350
Stanford University	3	Female	Pontine diffuse midline glioma	XRT	No	Censored at 98
Stanford University	16	Male	Pontine diffuse midline glioma	XRT, panobinostat	No	393
Stanford University	6	Female	Pontine diffuse midline glioma	XRT, panobinostat x1 dose	No	266
Stanford University	6	Male	Pontine diffuse midline glioma, H3K27-altered	XRT, TMZ, Subtotal resection, CCNU, pomalidomide, oral cyclophosphamide, oral topotecan	No	395
Stanford University	8	Male	Pontine diffuse midline glioma, H3K27-altered	XRT, panobinostat	No	176
Stanford University	2	Male	Pontine diffuse midline glioma	XRT	No	385

Stanford University	6	Male	Pontine diffuse midline glioma	XRT	No	Censored at 39
Stanford University	7	Male	Pontine diffuse midline glioma, H3K27-altered	XRT	No	185
Stanford University	5	Male	Pontine diffuse midline glioma, H3K27-altered	XRT	No	Censored at 187
Stanford University	10	Male	Pontine diffuse midline glioma	XRT, ONC201	No	190
Stanford University	2	Male	Pontine diffuse midline glioma	XRT	No	462
Stanford University	5	Male	Pontine diffuse midline glioma, H3WT, TP53 loss and point mutation, PDGFR loss, HDAC3 loss, CDK1 gain, CLK4 loss, MAPK7 loss, MYLK loss, TGFBR2 loss, GSK3B loss, PSMB5 gain, PIK3CB loss, HSPBAP1 loss, MDM2 gain, AURKB loss	XRT (only two fractions)	No	217
Stanford University	1	Male	Pontine diffuse midline glioma	XRT, Cisplatin, Cyclophosphamide, Etoposide, Vincristine	No	792
Stanford University	4	Female	Pontine diffuse midline glioma	XRT, Etoposide	No	410
Stanford University	8	Female	Pontine diffuse midline glioma	XRT, Etoposide, Topotecan	No	646
Stanford University	9	Female	Pontine diffuse midline glioma	XRT, TMZ, Etoposide, Thalidomide	No	514
Stanford University	5	Male	Pontine diffuse midline glioma	XRT	No	230
Stanford University	5	Female	Pontine diffuse midline glioma	XRT	No	255
Stanford University	4	Female	Pontine diffuse midline glioma	XRT, Cyclosporine, Etoposide, Vincristine	No	291
Stanford University	5	Female	Pontine diffuse midline glioma	XRT	No	255
Stanford University	4	Male	Pontine diffuse midline glioma	XRT	No	314
Stanford University	6	Female	Pontine diffuse midline glioma	XRT, Cyclosporine, Etoposide, Vincristine	No	222
Stanford University	5	Female	Pontine diffuse midline glioma	XRT, Etoposide, Vincristine	No	295
Stanford University	5	Male	Pontine diffuse midline glioma	XRT, Etoposide	No	305

Stanford University	11	Male	Pontine diffuse midline glioma	XRT, Etoposide, Vincristine	No	115
Stanford University	6	Female	Pontine diffuse midline glioma	XRT, Etoposide, Vincristine	No	218
Stanford University	5	Male	Pontine diffuse midline glioma	XRT, Gadolinium texaphyrin	No	273
Stanford University	4	Female	Pontine diffuse midline glioma	XRT, TMZ	No	190
Stanford University	5	Female	Pontine diffuse midline glioma	XRT, TMZ	No	302
Stanford University	6	Female	Pontine diffuse midline glioma	XRT	No	336
Stanford University	8	Female	Pontine diffuse midline glioma	XRT	No	434
Stanford University	7	Female	Pontine diffuse midline glioma	XRT, Gadolinium texaphyrin	No	353
Stanford University	5	Male	Pontine diffuse midline glioma	XRT	No	160
Stanford University	12	Male	Pontine diffuse midline glioma	XRT	No	Censored at 225
Stanford University	3	Male	Pontine diffuse midline glioma, H3K27-altered	XRT, panobinostat	No	Censored at 427

Legend:
XRT = radiation
TMZ = temozolomide
COG = Children's Oncology Group

Extended Data Table 2. Hemispheric High Grade Glioma Patients

Institution	Age (years)	Sex	Diagnosis	Other treatments	Levetiracetam yes/no	Overall survival (days)
University of Michigan	0.6	Female	Glioblastoma (glioblastoma multiforme, astrocytoma WHO IV), SETD2 S396* mutation, PDGFB amplification (19 copies), H3WT	XRT, TMZ, cisplatin, cyclophosphamide, etoposide, vincristine, dasatinib, Tandem transplant, Subtotal Resection	Yes	871
University of Michigan	16	Male	Cortical/hemispheric astrocytoma, PDGFRA mutant, H3WT	XRT, TMZ, Tripleptal, Vimpat, Dasatanib/Everolimus	Yes	1016
University of Michigan	9	Female	Cortical glioblastoma, TP53 P152L, TP53: Splice donor of exon 4 ATRX R1022* (monoallelic), PRMT2 D95G, Aneuploid CDK4 amplification (chr12; 8 copies), SMARCD1 amplification (chr12; 8 copies), NCOR2 amplification (chr12; 10 copies)	Subtotal resection	Yes	753
University of Michigan	7	Female	Craniopharyngioma (adamantinomatous), CTNNB1 T41I, activating IQGAP3 S1406N	Subtotal Resection	Yes	Censored at 12
University of Michigan	8	Male	Glioblastoma (glioblastoma multiforme, astrocytoma WHO IV), Hypermutation (401.9 Mutations/Mb): TP53 R248W, R158, HDICER1 E1705K, MAP4K3 M1, AMER1 R358*, BCOR R1513*, CTNNA2 R882*, CTNNA1 R451*, IDH1 R100*, KMT2A R407*, PTPN2 R354*, NF1 E2207*, ATM I1581fs, BAX E41fs, FLG E160fs, SOS1 L518fs, NR4A2 Q109fs, KMT2C F835fs, Copy gain chr5 (p15.3-p13.2); Copy loss chr4 (q13.1-q22.1)	XRT, proton XRT, TMZ, bevacuzimab, vorinostat, Valproic acid, cytox, doxorubicin, vincristine, ara-c, methotrexate, pembrolizumab, Subtotal Resection	Yes	3285
University of Michigan	18	Female	Anaplastic pleomorphic xanthoastrocytoma, BRAF V600ETP53 AC276GG, NUTM2F R176G, IRS4 Y828*, PKHD1 A3742V, Genome-wide polyploidy CDKN2A/2B homozygous deletion	Proton XRT, Debrafenib, trametinib, Subtotal Resection	Yes	Censored at 959
University of Michigan	15	Male	Anaplastic astrocytoma, IDH1 R123H-negative, 17.7 Mutations/Mb	Proton XRT, Pembrolizumab, Bevacuzimab, vimpat	Yes	480

			Microsatellite instability (MSI) signature noted TP53 R273C, PTPN11 A72V, PIK3CA Q546R, MITF R110* stopgain, NF1 D2346fs, NF1 G675fs, MSH3 K383fs, WRN E510del, Additional frame-shift mutations: CBX5 K106fs, PDS5B K1318fs, SETD1B H8fs, DDR1 P483fs, TET1 K23fs, SMC5 I939fs, SETD2 N1396fs, TET3 N351fs, copy loss chr14; copy gain chr17q			
University of Michigan	15	Male	Diffuse astrocytoma	XRT, TMZ, Everolimus, Lacosamide	Yes	233
University of Michigan	11	Male	Anaplastic astrocytoma, TP53 I195T, NF1 R440* stopgain, ERBB2 K831T, SCN5A E1060* stopgain, E1070Q, DOCK2 T1279M, ECT2L R233P, Amplifications: Chr3 (CTNNB1, ETV5, SOX2); chr13 (IRS2)	XRT, TMZ, Depakote	Yes	82
University of Michigan	18	Male	Anaplastic astrocytoma (astrocytoma WHO III), ATRX R2178G, PTPN11 Q510L, MYH11 R449Q, E2F1 R166C, POU5F1B R230Q, MYB amplification (exon 1 to 9), Copy loss chr1p-ter, 3p, 2p; UPD chr11p	Vimpat, Gross Total Resection	Yes	Censored at 572
University of Michigan	16	Female	Glioblastoma (glioblastoma multiforme, astrocytoma WHO IV), H3.3 G34R, ATRX E1461* stopgain, GRM3 L91F, PDGFRA P250S, TP53 D186fs insertion, Aneuploidy (polyploidy)	XRT, TMZ, lomustine, Subtotal Resection	Yes	Censored at 309
University of Michigan	18	Male	Anaplastic astrocytoma (astrocytoma WHO III), ATRX S1379* stopgain, NRG3 P289H, CDKN2A/2B deletion, PTPRM deletion, PTPN2 deletion, Copy loss: chr1p, 5q, 11q, 13, 14 UPD: chr17p (TP53), chr4q, 20p	XRT, TMZ, Irinotecan, Palbociclib, Subtotal Resection	Yes	165
University of Michigan	1	Female	Anaplastic astrocytoma (astrocytoma WHO III)	Larotrectinib, Vigabatrin	Yes	Censored at 169
Stanford University	6	Female	Thalamic and medial temporal lobes anaplastic astrocytoma (astrocytoma WHO III)	XRT, TMZ, Lomustine	Yes	277

Stanford University	8	Female	Anaplastic astrocytoma (astrocytoma WHO III)	XRT, TMZ	Yes	404
Stanford University	12	Female	Anaplastic astrocytoma (astrocytoma WHO III)	XRT, TMZ, Topotecan, oral cyclophosphamide (5 days)	Yes	571
Stanford University	11	Female	Glioblastoma (glioblastoma multiforme, astrocytoma WHO IV)	Gross Total Resection	Yes	31
Stanford University	20	Male	Glioblastoma (glioblastoma multiforme, astrocytoma WHO IV)	XRT, TMZ, Bevacizumab	Yes	360
Stanford University	8	Male	Anaplastic astrocytoma (astrocytoma WHO III)	XRT, TMZ, Bevacizumab	Yes	262
Stanford University	15	Male	Glioblastoma (glioblastoma multiforme, astrocytoma WHO IV)	XRT, TMZ, Celocoxib, Lapatinib, Rindopepimut, GM-CSF, Subtotal Resection	Yes	649
Stanford University	7	Male	Glioblastoma (glioblastoma multiforme, astrocytoma WHO IV)	XRT, TMZ, Bevacizumab, Cyclophosphamide, Gross Total Resection	Yes	750
Stanford University	0.1	Female	Glioblastoma (glioblastoma multiforme, astrocytoma WHO IV)	Subtotal resection, TMZ, Carboplatin, Cisplatin, Cyclophosphamide, Eroltinib, Etoposide, Methotrexate, Topotecan, Vincristine, Bevacizumab, Irinotecan	Yes	Censored at 3529
Stanford University	17	Male	Glioblastoma (glioblastoma multiforme, astrocytoma WHO IV)	XRT, TMZ, Bevacizumab	Yes	432
Stanford University	15	Male	Glioblastoma (glioblastoma multiforme, astrocytoma WHO IV)		Yes	Censored at 38
Stanford University	2	Male	Glioblastoma (glioblastoma multiforme, astrocytoma WHO IV), H3WT	Carboplatin, Cisplatin, Cyclophosphamide, Erlotinib, Etoposide, Methotrexate, Topotecan, Vincristine, Gross Total Resection	Yes	Censored at 2504
Stanford University	24	Female	Glioblastoma (glioblastoma multiforme, astrocytoma WHO IV)	XRT, TMZ, Bevacizumab, Cyberknife, Carmustine, Erlotinib, Gross Total Resection	Yes	525
Stanford University	2	Male	Glioblastoma (glioblastoma multiforme, astrocytoma WHO IV)	Subtotal Resection	Yes	107
Stanford University	12	Female	Glioblastoma (glioblastoma multiforme, astrocytoma WHO IV)	XRT, TMZ, Bevacizumab, etoposide, Subtotal Resection	Yes	709
Stanford University	1	Male	Glioblastoma (glioblastoma multiforme, astrocytoma WHO IV)	Carboplatin, Cisplatin, Cyclophosphamide, Eroltinib, Etoposide, Methotrexate,	Yes	Censored at 2284

				Topotecan, Vincristine, Gross Total Resection		
Stanford University	10	Female	Anaplastic astrocytoma (astrocytoma WHO III)	XRT, TMZ, Bevacizumab, Carmustine, Irinotecan	Yes	Censored at 1093
Stanford University	18	Female	Glioblastoma (glioblastoma multiforme, astrocytoma WHO IV)	XRT, TMZ	Yes	122
Stanford University	12	Female	Glioblastoma (glioblastoma multiforme, astrocytoma WHO IV)	XRT, Cisplatin, Cyclophosphamide, Etoposide, Vincristine, cabazitaxel, Subtotal resection	Yes	Censored at 1112
Stanford University	0.3	Male	Glioblastoma (glioblastoma multiforme, astrocytoma WHO IV)	Cisplatin, Cyclophosphamide, Vincristine, topotecan, erlotinib, Gross Total Resection	Yes	Censored at 1210
Stanford University	15	Male	Glioblastoma (glioblastoma multiforme, astrocytoma WHO IV)	XRT, TMZ, CCNU, Bevacizumab, subtotal resection	Yes	732
Stanford University	7	Male	Anaplastic astrocytoma (astrocytoma WHO III)	XRT, TMZ, Bevacizumab, Optune, Irinotecan, Subtotal Resection	Yes	1360
Stanford University	18	Female	Glioblastoma (glioblastoma multiforme, astrocytoma WHO IV)	XRT, TMZ, Bevacizumab, Erlotinib, Near Total Resection	Yes	312
Stanford University	3	Male	Pilocytic astrocytoma (WHO I), relapsed as anaplastic astrocytoma (WHO III)	XRT, TMZ, Bleomycin, P-32, gross total resection	Yes	Censored at 9280
Stanford University	17	Female	Anaplastic astrocytoma (astrocytoma WHO III)	XRT, subtotal resection, TMZ, Bevacizumab, Irinotecan	Yes	1033
Stanford University	11	Female	Anaplastic astrocytoma (astrocytoma WHO III)	XRT, TMZ, Etoposide, Irinotecan, Oxaliplatin, Subtotal Resection	Yes	866
Stanford University	0.4	Female	Glioblastoma (glioblastoma multiforme, astrocytoma WHO IV), H3WT	Antineoplastons, etoposide, Bevacizumab, Gross Total Resection	Yes	Censored at 432
Stanford University	20	Female	Glioblastoma (glioblastoma multiforme, astrocytoma WHO IV)	XRT, TMZ, Gross Total Resection	Yes	Censored at 70
University of Michigan	14	Male	Right Parietal Glioblastoma Multiforme, somatic TSC2 R611W mutation, homozygous deletion of PAK1, germline loss of TP53	Proton XRT, everolimus, Gross total resection	No	Censored at 1953
University of Michigan	16	Female	Glioblastoma multiforme, PDGFRRA V536E and P577R, STAG2 R263W	XRT, dasatinib, etoposide, subtotal resection	No	Censored at 203
University of Michigan	15	Male	Pleomorphic, xanthoastrocytoma, grade 2, BRAF V600E positive	Proton XRT, subtotal resection	No	Censored at 836
University of Michigan	7	Female	Anaplastic ependymoma, PF-EPN-A, 1q and 5p gain	Proton XRT, Gross total resection	No	Censored at 811

Stanford University	20	Male	Anaplastic astrocytoma (astrocytoma WHO III)	XRT, Carboplatin, Lomustine, Procarbazine, Vincristine	No	417
Stanford University	10	Male	Anaplastic astrocytoma (astrocytoma WHO III)	XRT, TMZ, Etoposide, Thalidomide, Subtotal Resection	No	252
Stanford University	0.8	Male	Glioblastoma (glioblastoma mutliforme, astrocytoma WHO IV)	Etoposide, Subtotal Resection	No	146
Stanford University	16	Male	Anaplastic astrocytoma (astrocytoma WHO III)	XRT, TMZ, Subtotal Resection	No	Censored at 57
Stanford University	17	Male	Glioblastoma (glioblastoma multiforme, astrocytoma WHO IV)	XRT, TMZ, Oxaliplatin, Subtotal Resection	No	Censored at 386
Stanford University	15	Female	Glioblastoma (glioblastoma multiforme, astrocytoma WHO IV)	XRT, TMZ, Subtotal Resection	No	Censored at 61
Stanford University	2	Female	Anaplastic astrocytoma (astrocytoma WHO III)	Gross Total Resection	No	Censored at 26
Stanford University	17	Female	Anaplastic astrocytoma (astrocytoma WHO III), H3WT	XRT, Subtotal Resection	No	Censored at 411
Stanford University	4	Male	Anaplastic astrocytoma (astrocytoma WHO III)	Gross Total Resection	No	Censored at 32
Stanford University	9	Female	Glioblastoma (glioblastoma multiforme, astrocytoma WHO IV)	XRT, TMZ	No	25
Stanford University	14	Male	Glioblastoma (glioblastoma multiforme, astrocytoma WHO IV)	XRT, TMZ, Lomustine, Subtotal Resection	No	285
Stanford University	0	Male	Glioblastoma (glioblastoma multiforme, astrocytoma WHO IV)	TMZ, Lomustine, Subtotal Resection	No	Censored at 17
Stanford University	17	Female	Thalamic glioblastoma (glioblastoma multiforme, astrocytoma WHO IV)	XRT, TMZ, Lomustine, Bevacizumab	No	837
Stanford University	16	Female	Glioblastoma (glioblastoma multiforme, astrocytoma WHO IV)	XRT, TMZ, Carboplatin, Cisplatin, Cyclophosphamide, Vincristine, Bevacizumab, Irinotecan, Subtotal Resection	No	Censored at 2067
Stanford University	13	Female	Posterior fossa glioblastoma (glioblastoma multiforme, astrocytoma WHO IV)	XRT, TMZ, Bevacizumab, Imatinib mesylate	No	523
Stanford University	11	Female	Glioblastoma (glioblastoma multiforme, astrocytoma WHO IV)	XRT, TMZ, Bevacizumab, Subtotal Resection, BCNU, irinotecan	No	705
Stanford University	10	Male	Glioblastoma (glioblastoma multiforme, astrocytoma WHO IV)	XRT, TMZ, Bevacizumab, Cediranib, Carmustine, Irinotecan, Gross Total Resection	No	518
Stanford University	9	Female	Pontine and cerebellar anaplastic astrocytoma (astrocytoma WHO III)	XRT, Arsenic Trioxide	No	Censored at 220

Stanford University	11	Female	Glioblastoma (glioblastoma multiforme, astrocytoma WHO IV)	XRT, TMZ, Arsenic Trioxide, Bevacizumab, Irinotecan, Cyclophosphamide, subtotal resection	No	424
Stanford University	16	Male	Anaplastic astrocytoma (astrocytoma WHO III), H3WT	XRT, TMZ, Subtotal Resection	No	Censored at 3893
Stanford University	6	Male	Glioblastoma (glioblastoma multiforme, astrocytoma WHO IV)	NA	No	Censored at 12
Stanford University	0	Female	Glioblastoma (glioblastoma multiforme, astrocytoma WHO IV)	Subtotal Resection	No	1
Stanford University	11	Female	Anaplastic astrocytoma (astrocytoma WHO III)	XRT, TMZ, Bevacizumab, Etoposide	No	258
Stanford University	9	Male	Glioblastoma (glioblastoma multiforme, astrocytoma WHO IV)	XRT, TMZ, Bevacizumab	No	333
Stanford University	9	Female	Glioblastoma (glioblastoma multiforme, astrocytoma WHO IV)	XRT, TMZ, Bevacizumab, Lomustine, Gross Total Resection	No	Censored at 331
Stanford University	7	Female	Thalamic anaplastic astrocytoma (astrocytoma WHO III)	XRT, TMZ, Carboplatin, Vincristine	No	Censored at 308
Stanford University	2	Female	Glioblastoma (glioblastoma multiforme, astrocytoma WHO IV), H3WT	XRT, TMZ, Vorinostat, Gross Total Resection	No	Censored at 556
Stanford University	11	Female	Diffuse astrocytoma (astrocytoma WHO II)	Gross Total Resection	No	Censored at 1475
Stanford University	4	Female	Anaplastic astrocytoma (astrocytoma WHO III)	Gross Total Resection	No	Censored at 4830
Stanford University	9	Female	Anaplastic astrocytoma (astrocytoma WHO III)	XRT, TMZ, Lomustine	No	Censored at 249
Stanford University	*in utero* (at 36-week ultrasound)	Female	Glioblastoma (glioblastoma multiforme, astrocytoma WHO IV), H3WT, IDH WT	Etoposide, Carboplatin, Cyclophosphamide, Vincristine	No	Censored at 883
Stanford University	5	Female	Glioblastoma (glioblastoma multiforme, astrocytoma WHO IV), H3K27-altered		No	Censored at 161
Stanford University	2	Male	Mixed malignant germ cell tumor	XRT, Carboplatin, Etoposide, Ifosfamide, Subtotal Resection	No	187
Stanford University	0.6	Male	Anaplastic astrocytoma (astrocytoma WHO III)	Subtotal Resection	No	Censored at 30
Stanford University	0.7	Female	Glioblastoma (glioblastoma multiforme, astrocytoma WHO IV), H3WT	Cisplatin, Cyclophosphamide, Methotrexate, Vincristine	No	Censored at 262

Stanford University	11	Female	Anaplastic ependymoma	XRT, Carboplatin, Cyclophosphamide, Etoposide, Vincristine	No	Censored at 107
Stanford University	2	Female	Anaplastic astrocytoma (astrocytoma WHO III), H3WT	Carboplatin, Vinblastine, Vincristine	No	Censored at 281
Stanford University	7	Female	Anaplastic astrocytoma (astrocytoma WHO III)	XRT, Cisplatin	No	176
Stanford University	6	Male	Anaplastic astrocytoma (astrocytoma WHO III)	XRT, Cisplatin, Subtotal Resection	No	157
Stanford University	9	Male	Glioblastoma (glioblastoma multiforme, astrocytoma WHO IV)	Carmustine, Etoposide, 6-thioguanine, Subtotal Resection	No	86
Stanford University	5	Female	Anaplastic astrocytoma (astrocytoma WHO III)	XRT, Carboplatin, Etoposide, Ifosfamide	No	Censored at 308
Stanford University	10	Male	Glioblastoma (glioblastoma multiforme, astrocytoma WHO IV)	XRT, TMZ, Celocoxib, Subtotal Resection	No	Censored at 53
Stanford University	13	Male	Glioblastoma (glioblastoma multiforme, astrocytoma WHO IV)	XRT, Lomustine, Procarbazine, Vincristine, Etoposide, Subtotal Resection	No	894
Stanford University	17	Female	Glioblastoma (glioblastoma multiforme, astrocytoma WHO IV)	XRT, TMZ, Carmustine, Imatinib mesylate	No	676
Stanford University	17	Female	Glioblastoma (glioblastoma multiforme, astrocytoma WHO IV)	XRT, TMZ	No	293
Stanford University	14	Male	Glioblastoma (glioblastoma multiforme, astrocytoma WHO IV)	XRT, TMZ, Lomustine, Procarbazine, Vincristine, Thalidomide, Subtotal Resection	No	1993
Stanford University	12	Female	Glioblastoma (glioblastoma multiforme, astrocytoma WHO IV)	XRT, Lomustine, Procarbazine, Vincristine, Gross Total Resection	No	Censored at 4976
Stanford University	4	Male	Glioblastoma (glioblastoma multiforme, astrocytoma WHO IV)	Subtotal Resection	No	51
Stanford University	13	Male	Astrocytoma (anaplastic vs pleomorphic xanthoastrocytoma)	XRT, TMZ, Gross Total Resection	No	Censored at 3007
Stanford University	7	Female	Anaplastic astrocytoma (astrocytoma WHO III)	XRT, Carmustine, Cisplatin, Topotecan, Subtotal Resection	No	347
Stanford University	1	Female	Anaplastic astrocytoma (astrocytoma WHO III)	XRT, TMZ, Thalidomide	No	3852
Stanford University	2	Female	Gliosarcoma	XRT, Carmustine, O-6-benzylguanine, Subtotal Resection	No	222
Stanford University	8	Female	Anaplastic astrocytoma (astrocytoma WHO III)	XRT, TMZ, Carmustine, O-6-benzylguanine	No	279

Stanford University	2	Male	Diffuse astrocytoma (WHO II), then glioblastoma (glioblastoma multiforme, astrocytoma WHO IV)	XRT, TMZ, Subtotal Resection, bevacizumab, regorafenib, palbociclib, savolitinib	No	6957
Stanford University	7	Male	Anaplastic astrocytoma (astrocytoma WHO III)	XRT, TMZ, Imatinib mesylate, Subtotal Resection	No	263

Legend:
XRT = radiation
TMZ = temozolomide